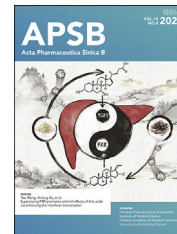




Chinese Pharmaceutical Association
Institute of Materia Medica, Chinese Academy of Medical Sciences

Acta Pharmaceutica Sinica B

www.elsevier.com/locate/apbs
www.sciencedirect.com



ORIGINAL ARTICLE

Discovery of first-in-class DOT1L inhibitors against the R231Q gain-of-function mutation in the catalytic domain with therapeutic potential of lung cancer



Zehui Tan^{a,†}, Ning Guo^{b,†}, Zhi Cao^a, Shuyu Liu^a, Jiayu Zhang^b,
Deyi Ma^a, Jiahao Zhang^a, Wencai Lv^b, Nan Jiang^a, Linghe Zang^b,
Lihui Wang^{b,*}, Xin Zhai^{a,*}

^aKey Laboratory of Structure-Based Drug Design and Discovery, Ministry of Education, Shenyang Pharmaceutical University, Shenyang 110016, China

^bDepartment of Pharmacology, Shenyang Pharmaceutical University, Shenyang 110016, China

Received 19 January 2024; received in revised form 18 February 2024; accepted 1 March 2024

KEY WORDS

DOT1L;
R231Q mutation;
Lung cancer;
Adenosine-containing
inhibitors;
Epigenetics

Abstract Recent research certified that DOT1L and its mutations represented by R231Q were potential targets for the treatment of lung cancer. Herein, a series of adenosine-containing derivatives were identified with DOT1L^{R231Q} inhibition through antiproliferation assay and Western blot analysis in the H460^{R231Q} cell. The most promising compound **37** significantly reduced DOT1L^{R231Q} mediated H3K79 methylation and effectively inhibited the proliferation, self-renewal, migration, and invasion of lung cancer cell lines at low micromolar concentrations. The cell permeability and cellular target engagement of **37** were verified by both CETSA and DARTS assays. In the H460^{R231Q} OE cell-derived xenograft (CDX) model, **37** displayed pronounced tumor growth inhibition after intraperitoneal administration at 20 mg/kg dose for 3 weeks (TGI = 54.38%), without obvious toxicities. A pharmacokinetic study revealed that **37** possessed tolerable properties ($t_{1/2} = 1.93 \pm 0.91$ h, $F = 97.2\%$) after intraperitoneal administration in rats. Mechanism study confirmed that **37** suppressed malignant phenotypes of lung cancer carrying R231Q gain-of-function mutation *via* the MAPK/ERK signaling pathway. Moreover, analysis of the binding modes between molecules and DOT1L^{WT/R231Q} proteins put forward the “Induced-fit” allosteric model in favor to the discovery of potent DOT1L candidates.

*Corresponding authors.

E-mail addresses: lhwang@syphu.edu.cn (Lihui Wang), zhaixin_syphu@126.com (Xin Zhai).

[†]These authors made equal contributions to this work.

Peer review under the responsibility of Chinese Pharmaceutical Association and Institute of Materia Medica, Chinese Academy of Medical Sciences.

<https://doi.org/10.1016/j.apbs.2024.03.018>

2211-3835 © 2024 The Authors. Published by Elsevier B.V. on behalf of Chinese Pharmaceutical Association and Institute of Materia Medica, Chinese Academy of Medical Sciences. This is an open access article under the CC BY-NC-ND license (<http://creativecommons.org/licenses/by-nc-nd/4.0/>).

© 2024 The Authors. Published by Elsevier B.V. on behalf of Chinese Pharmaceutical Association and Institute of Materia Medica, Chinese Academy of Medical Sciences. This is an open access article under the CC BY-NC-ND license (<http://creativecommons.org/licenses/by-nc-nd/4.0/>).

1. Introduction

Histone methylation is a critical post-translational modification process mediated by histone methyltransferases¹. Disruptor of telomeric silencing 1-like (DOT1L) is the only known H3K79 methyltransferase in histone lysine methyltransferases². Due to its key role in leukemogenesis, DOT1L as an attractive therapeutic target of MLL-rearranged leukemia has been studied for a dozen years, resulting in the identification of abundant DOT1L inhibitors^{3,4}. With further research, it has been validated that aberrant expression of DOT1L is associated with various tumorigenesis, including breast cancer^{5,6}, prostate cancer^{7,8}, ovarian cancer^{9,10}, gastric cancer¹¹, colorectal cancer¹², and lung cancer¹³.

Over the past decades, continuous research in lung cancer therapy led to the identification of a variety of therapeutic targets, such as traditional EGFR and ALK along with novel underexploited DOT1L^{14,15}. DOT1L-mediated H3K79 methylation was dramatically up-regulated in tumor lung tissues compared to normal lung tissues isolated from clinical patients with adenocarcinoma or squamous cell carcinoma, while the knockdown of DOT1L in A549 and NCI-H1299 human lung cancer cells resulted in inhibition of cell proliferation, premature senescence and cell cycle arrest at G₁ phase¹⁶. In a study to identify novel drivers of lung carcinogenesis, DOT1L was disclosed as a markedly mutated gene in lung adenocarcinoma, with mutation rate about 3%¹⁷. Furthermore, according to the TCGA database¹⁸, DOT1L mutations also contributed to halved overall survival and poor prognosis in lung cancer patients. Most recently, a series of gain-of-function mutations in the catalytic domain of DOT1L was identified in lung cancer by our group, especially represented by the R231Q mutation with stronger enzymatic activity and ligand affinity^{19,20}. Lung cancer cell lines carrying the R231Q mutation exhibited comprehensively enhanced malignant phenotypes, such as proliferation, self-renewal, invasion, metastasis, and drug resistance. Similar oncogenicity of the R231Q mutation was observed *in vivo*, identified by the fact that the tumor weight and volume in the mutant group were prominently higher than that in the wild-type (WT) group. Mechanistically, DOT1L^{R231Q} specifically activated the MAPK/ERK signaling pathway by enriching H3K79me2 on the *RAF1* promoter and epigenetically regulating the expression of downstream targets such as *ELK3* and *KLF4*¹⁹, thereby contributing to the malignancy of lung cancer (Fig. 1). Consequently, DOT1L and its mutation as triggers of lung carcinogenesis provided new potential targets for lung cancer therapy.

Previous study found a larger SAM binding pocket in DOT1L^{R231Q} than in DOT1L^{WT}, accounting for the enhanced enzymatic activity and ligand affinity of R231Q mutant protein along with the drug resistance against DOT1L^{WT} inhibitors¹⁹. Resultantly, none of DOT1L^{WT} inhibitors including SGC0946²¹, EPZ004777²² and EPZ5676²³ effectively inhibited the proliferation of H460 cells expressing DOT1L^{R231Q} (Fig. 2). The optimal SGC0946 displayed obviously weaker inhibition against R231Q group (H460^{R231Q} IC₅₀ = 38.00 μmol/L, TGI = 26.5%)

compared with its inhibitory activity against WT group both *in vitro* and *in vivo* (H460^{WT} IC₅₀ = 9.18 μmol/L, TGI = 44.4%)¹⁹, thereby motivating us to develop novel DOT1L inhibitors against the R231Q gain-of-function mutation. In this work, based on the enlarged cavity of the SAM binding site within R231Q mutant protein, we launched a development program for DOT1L^{R231Q} inhibitors with different skeletons and central N-side chains, and the promising results were presented in the following.

2. Results and discussion

2.1. Structure–activity relationship (SAR) study

Structurally, the catalytic domain of DOT1L^{WT} (aa 1–416) comprises N-lobe (aa 1–126), C-lobe (aa 141–332), SAM-binding loop (aa 127–140) and substrate-binding loop (aa 301–311)²⁴. Consistent with previous report¹⁹, molecular dynamics simulations disclosed an enlarged cavity at the SAM binding site in DOT1L^{R231Q}, especially around the sulfur atom of ligand SAM (Fig. 3). Additionally, both SGC0946 and EPZ004777 showed better potency against R231Q mutation than EPZ5676, implying that the urea moiety might be an important pharmacophore. Hence, based on SGC0946, novel DOT1L^{R231Q} inhibitors were designed through the following three strategies: (1) the adenosine head was retained for that it could form four vital hydrogen bonds with residues Glu186, Asp222 and Phe223, anchoring the entire molecule in the SAM binding site; (2) the *n*-propyl linker of SGC0946 was replaced by the bulky bicyclic linker to adequately fill the enlarged cavity around the sulfur atom of SAM; (3) reserving the urea moiety and introducing various substituted phenyl group, anticipating to form more interactions (Fig. 4).

Accordingly, compounds **1–5** bearing octahydrocyclopenta[*c*]pyrrole linker were designed and their antiproliferative effects on NCI-H460-DOT1L-WT/R231Q cells were evaluated *in vitro* (Table 1). Compared with **1** containing methyl group on the central nitrogen atom (R₁), compound **2** with isopropyl group displayed better inhibition against H460^{R231Q} cells, suggesting an obvious effect of central N-substituent (R₁) on potency. Besides, **2–5** with different substituted phenyl groups (R₂) were found to inhibit the proliferation of H460^{R231Q} cells, proving the feasibility of introducing a bulky bicyclic linker strategy. However, the incorporation of octahydrocyclopenta[*c*]pyrrole linker (**1–5**) decreased even vanished the antiproliferation against H460^{WT} cells, which might be attributed to the excessive rigidity caused by the combination of bicyclic rings and urea segment. Therefore, derivatives **6–11** were obtained by replacing the urea moiety with more flexible methylene. Unexpectedly, little inhibition against H460^{WT} cells was observed from **6–11**, indicating the bulky size rather than the rigidity of bicyclic rings impaired the binding between inhibitors and the relatively small SAM binding pocket of DOT1L^{WT}. Since none of compounds **1–11** showed antiproliferative activity against the H460^{WT} cell, subsequent *in vitro*

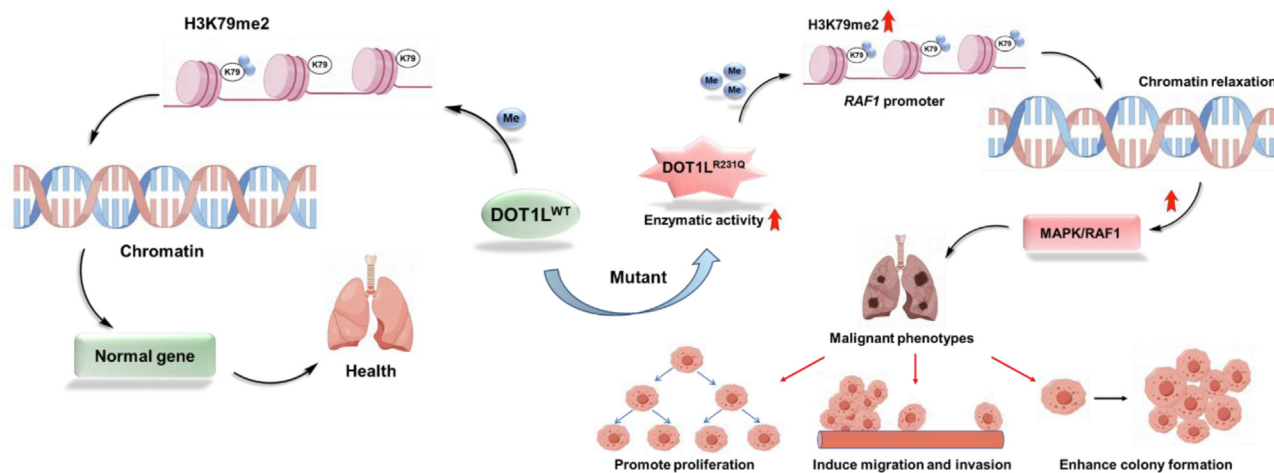


Figure 1 Summary diagram describing that gain-of-function DOT1L mutations promote the malignant phenotypes of lung cancer by regulating the MAPK/ERK signaling pathway¹⁹.

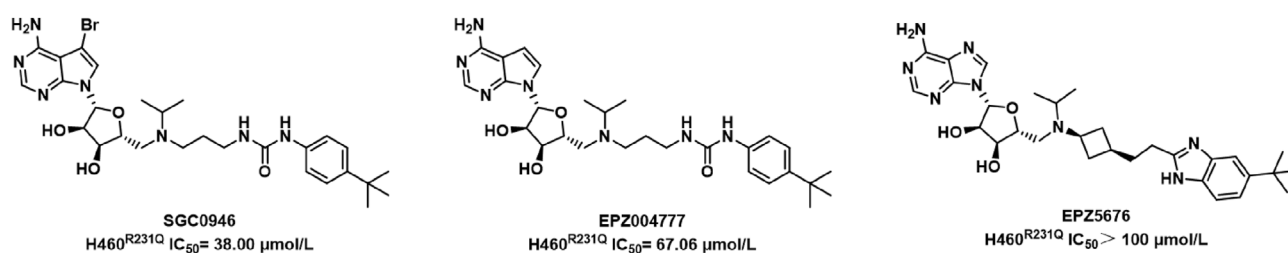


Figure 2 The chemical structures of representative DOT1L^{WT} inhibitors and their inhibitory activity against H460^{R231Q} cells.

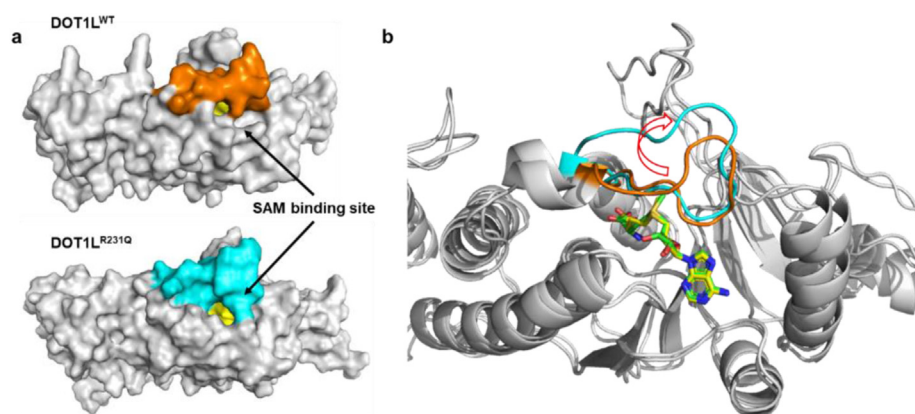


Figure 3 (a) Cocystal structure of DOT1L^{WT} (PDB ID: 1NW3) and predicted three-dimensional diagrams of DOT1L^{R231Q} at 100 ns obtained from molecular dynamics simulation, the cavities of SAM binding site are colored yellow, the SAM binding loops of DOT1L^{WT} and DOT1L^{R231Q} are colored orange and cyan, respectively. (b) Superposition of DOT1L^{WT} (ligand SAM yellow, SAM binding loop orange, protein gray) on DOT1L^{R231Q} (ligand SAM green, SAM binding loop cyan, protein gray) clarifies that R231Q mutation induces conformational rearrangement of SAM binding loop, leading to a larger cavity at the SAM binding site.

screening was performed based on the H460^{R231Q} cell, and additional trials were required to comprehensively determine the efficacy of tested compounds. Correspondingly, the quantitative Western blot (WB) analysis of DOT1L substrate level H3K79me2, which was significantly enhanced in the H460^{R231Q} cell, was developed as an index for preliminary screening. Despite

weaker than SGC0946, preferred **5** displayed moderate inhibitory activity against DOT1L^{R231Q} in WB assay (Fig. 5). Noteworthy, **6** with methylene (H460^{R231Q} IC₅₀ = 47.69 μmol/L) inhibited proliferation of H460^{R231Q} cells at a similar level to **3** with urea moiety (H460^{R231Q} IC₅₀ = 48.77 μmol/L), manifesting various modifications of the linker were tolerated. Furthermore, the

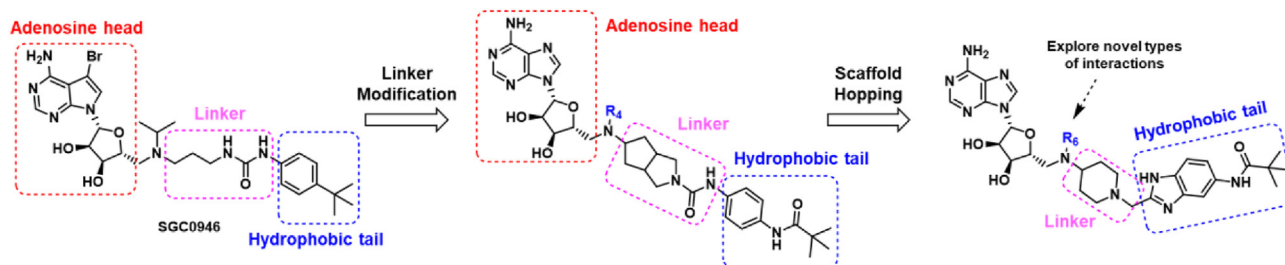
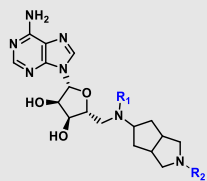


Figure 4 Rational design of DOT1L^{R231Q} inhibitors. The first series of DOT1L^{R231Q} inhibitors were designed based on the “three strategies” described above, and the second series of DOT1L^{R231Q} inhibitors were designed based on scaffold hopping and bioisosterism strategies.

Table 1 SAR exploration of compounds **1–11**.



Compd.	R ₁	R ₂	H460 ^{R231Q} (IC ₅₀ , μmol/L) ^a	H460 ^{WT} (IC ₅₀ , μmol/L) ^a
1	Me		77.56 ± 3.18	> 100
2	<i>i</i> Pr		40.15 ± 3.73	> 100
3	<i>i</i> Pr		48.77 ± 2.76	> 100
4	<i>i</i> Pr		60.04 ± 5.84	> 100
5	<i>i</i> Pr		37.91 ± 3.09	> 100
6	<i>i</i> Pr		47.69 ± 1.72	> 100
7	<i>i</i> Pr		73.46 ± 6.32	> 100
8	<i>i</i> Pr		85.78 ± 6.87	> 100
9	<i>i</i> Pr		> 100	> 100
10	<i>i</i> Pr		95.94 ± 4.26	> 100
11	<i>i</i> Pr		68.15 ± 3.03	> 100
SGC0946 ^b	—	—	38.00 ± 5.24	9.18 ± 0.11

^aDetermined in cell counting kit-8 (CCK-8) assay.

^bPositive control.

unsatisfied IC₅₀ values of compounds **8–11** against H460^{R231Q} cells revealed that di- or tri-substituents on the phenyl group (R₂) were adverse to the improved potency.

In view of the relatively high tolerance to modifications of the linker, a further SAR study emphasized on the length of the linker, thus driving the synthesis of **12–18** (Table 2). Dismayingly, all molecules (**12–18**) suffered a large loss in activity against the H460^{R231Q} cell. Compared with analogs **2–6**, the insertion of an additional ethyl group on octahydrocyclopenta[*c*]pyrrole linker led to an over 2-fold decrease in potency. Consistent with the

results of antiproliferation trials, **12–16** were unable to inhibit DOT1L^{R231Q} at 10 μmol/L in WB assay, with the observed H3K79me2 level even higher than that of the blank group (Fig. 5). A possible explanation for the abnormally elevated H3K79 dimethylation was that **12–16** might alter the rate of cell division or histone turnover which were mechanisms to counteract H3K79 methylation in the absence of H3K79 demethylase^{25,26}.

Aiming to investigate the effect of central N-substituent (R₄) on efficacy, derivatives **19–22** were obtained by replacing the isopropyl of **5** with an ester group or different amide groups

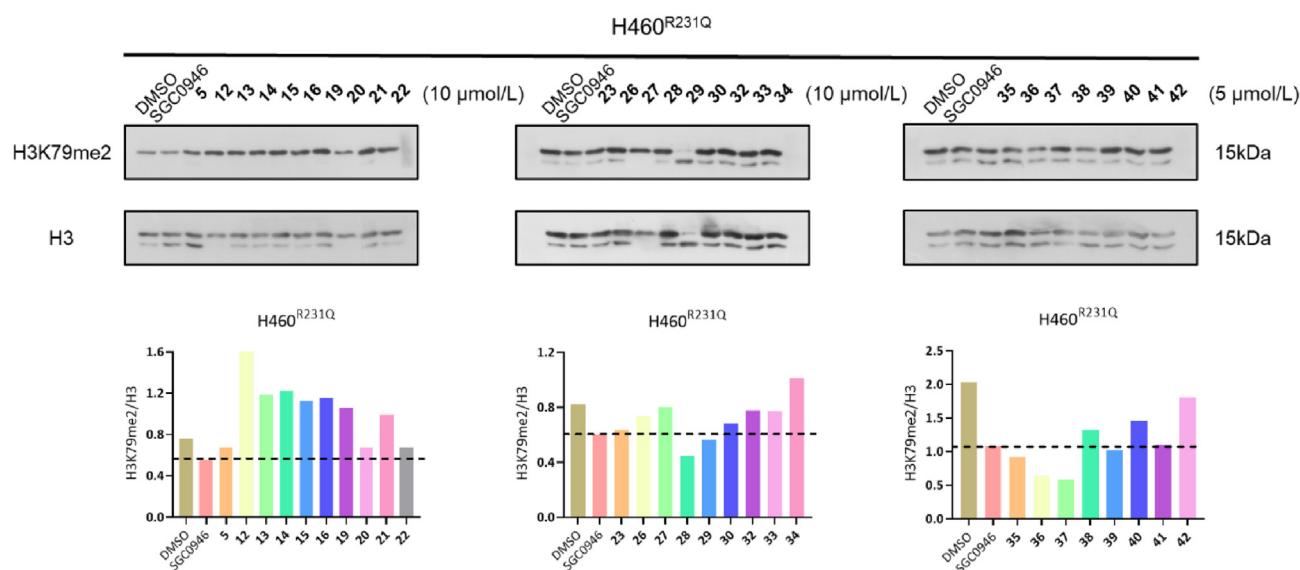


Figure 5 Initial screening of target compounds through quantitative WB analysis of the H3K79me2 level in H460^{R231Q} cells. Protein bands were quantified using Image J software, and the relative H3K79me2 levels were calculated by normalizing raw H3K79me2 measurements to histone H3 signals.

(Table 3). Delightfully, incorporation of a larger N-substituent (R₄) offered an alternative way to cope with larger SAM binding pocket caused by R231Q mutation, compounds **20** and **22** were found to be effective in reducing the expression of H3K79me2 in WB assay and in inhibiting the proliferation of H460^{R231Q} cells (Fig. 5). Notwithstanding, none of these

molecules were identified with more potent inhibition than SGC0946 in preliminary screening, motivating the reassessment of the skeleton. The rigidly linear conformation of **19–22** caused by the hexahydrocyclopenta[*c*]pyrrole-2(*1H*)-carboxamide linker possibly impeded the binding of inhibitors with DOT1L^{R231Q} protein, thereby limiting the improvement of activity.

Table 2 SAR exploration of compounds **12–18**.

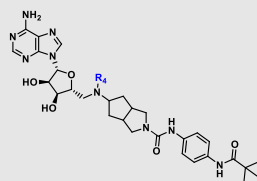
Compd.	R ₃	H460 ^{R231Q} (IC ₅₀ , μmol/L) ^a	Dimethylation index of H3K79 ^c
12		> 100	3.124
13		87.16 ± 7.63	2.128
14		> 100	2.187
15		> 100	2.029
16		96.59 ± 5.07	2.068
17		82.03 ± 3.25	ND ^d
18		> 100	ND ^d
SGC0946 ^b	—	38.00 ± 5.24	1

^aDetermined in cell counting kit-8 (CCK-8) assay.

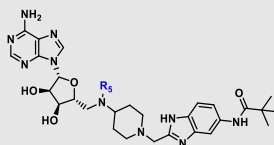
^bPositive control.

^cProtein bands in Fig. 5 were quantified using Image J software, and the relative H3K79me2 levels were calculated by normalizing raw H3K79me2 measurements to histone H3 signals. The dimethylation index of H3K79 was the ratio of Value_{compounds} to Value_{SGC0946}.

^dND refers to not determined.

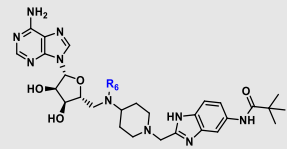
Table 3 SAR exploration of compounds **19–22**.

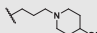
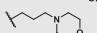
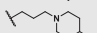
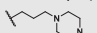
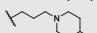
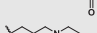
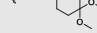
Compd.	R ₄	H460 ^{R231Q} (IC ₅₀ , μmol/L) ^a	Dimethylation index of H3K79 ^c
19		> 100	1.910
20		52.71 ± 2.99	1.218
21		72.50 ± 4.50	1.782
22		44.58 ± 3.87	1.209
SGC0946 ^b	—	38.00 ± 5.24	1

^aDetermined in cell counting kit-8 (CCK-8) assay.^bPositive control.^cProtein bands in Fig. 5 were quantified using Image J software, and the relative H3K79me2 levels were calculated by normalizing raw H3K79me2 measurements to histone H3 signals. The dimethylation index of H3K79 was the ratio of Value_{compounds} to Value_{SGC0946}.**Table 4** SAR exploration of compounds **23–35**.

Compd.	R ₅	H460 ^{R231Q} (IC ₅₀ , μmol/L) ^a	Dimethylation index of H3K79 ^c
23		34.76 ± 1.92	1.065
24		94.02 ± 7.07	ND ^d
25		69.95 ± 2.44	ND ^d
26		46.74 ± 2.69	1.230
27		46.68 ± 3.70	1.335
28		22.47 ± 1.81	0.747
29		29.16 ± 1.63	0.937
30		46.07 ± 3.00	1.138
31		> 100	ND ^d
32		96.51 ± 5.45	1.297
33		72.96 ± 5.07	1.287
34		59.35 ± 4.38	1.688
35		18.55 ± 0.94	0.854
SGC0946 ^b	—	38.00 ± 5.24	1

^aDetermined in cell counting kit-8 (CCK-8) assay.^bPositive control.^cProtein bands in Fig. 5 were quantified using Image J software, and the relative H3K79me2 levels were calculated by normalizing raw H3K79me2 measurements to histone H3 signals. The dimethylation index of H3K79 was the ratio of Value_{compounds} to Value_{SGC0946}.^dND refers to not determined.

Table 5 SAR exploration of compounds **36**–**42**.


Compd.	R ₆	H460 ^{R231Q} (IC ₅₀ , μmol/L) ^a	Dimethylation index of H3K79 ^c
36		8.76 ± 0.61	0.591
37		6.18 ± 0.55	0.536
38		43.07 ± 1.88	1.230
39		27.61 ± 1.31	0.944
40		55.29 ± 5.49	1.351
41		32.51 ± 3.56	1.019
42		73.33 ± 3.18	1.672
SGC0946 ^b	—	38.00 ± 5.24	1

^aDetermined in cell counting kit-8 (CCK-8) assay.^bPositive control.^cProtein bands in Fig. 5 were quantified using Image J software, and the relative H3K79me2 levels were calculated by normalizing raw H3K79me2 measurements to histone H3 signals. The dimethylation index of H3K79 was the ratio of Value_{compounds} to Value_{SGC0946}.

In pursuit of more potent inhibitors, scaffold optimization should be conducted on the hexahydrocyclopenta[*c*]pyrrole-2(1*H*)-carboxamide fragment. Utilizing the scaffold hopping and bioisosterism strategies, the hexahydrocyclopenta[*c*]pyrrole linker was replaced by a piperidine ring to reduce the rigidity (Fig. 4). Meanwhile, inspired by EPZ5676, the urea segment was incorporated into the benzene ring, finally affording compound **23** with novel skeleton. Encouragingly, **23** showed a better anti-proliferative effect on the H460^{R231Q} cell than SGC0946 along with comparable DOT1L^{R231Q} inhibition in WB assay (Fig. 5).

Based on **23**, a series of derivatives containing different N-substituents were developed and subsequently evaluated, including β-amide containing analogues **25**–**31** and γ-amide containing analogues **32**–**35** (Table 4). Compound **24** with an ester group exerted little inhibition of the H460^{R231Q} cell, neither did **19** bearing the same N-substituent. Conversion of the terminal

N,N-dimethyl amide (**25**) into pyrrolidino amide (**26**) or 4-methylpiperidino amide (**27**) resulted in increased efficacy toward H460^{R231Q} cells, suggesting sufficient space around the carbamoyl group. Delightfully, a favorable result was obtained by replacing 4-methyl of 4-methylpiperidino amide (**27**) with a polar hydroxyl (**28**), providing a potent inhibitor that surpassed SGC0946 in terms of both DOT1L^{R231Q} and H460^{R231Q} inhibition for the first time. Likewise, converting the terminal *N*-isopropyl amide (**33**) into dioxide-thiomorpholino amide (**34**) led to a little increased activity, and removing two oxygen atoms on dioxide-thiomorpholino ring furnished another potent compound **35**. These data suggested that the presence of a terminally polar atom on the N-substituent was conducive to enhancing the inhibition of DOT1L^{R231Q}. Meanwhile, the amide side chain with a suitable length could position the polar atom at the appropriate location to serve as a hydrogen-bond donor or acceptor. Inspired by **28** and

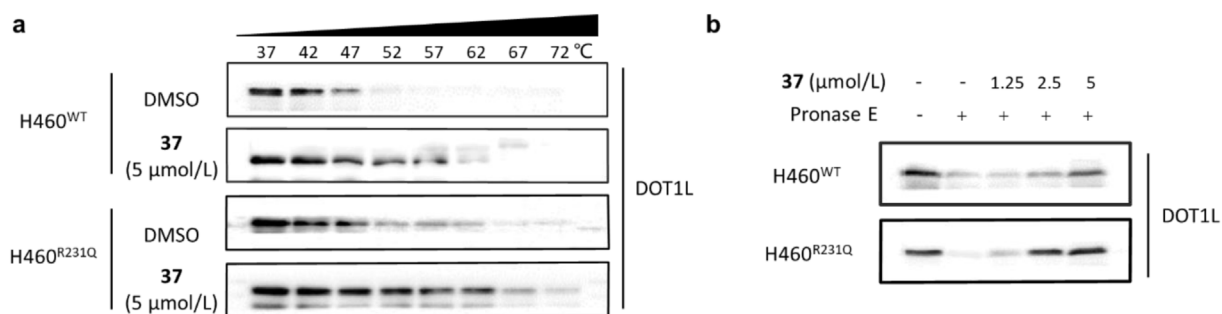


Figure 6 Cellular target engagement for compound **37**. (a) Cellular stabilization of DOT1L^{WT/R231Q} with 5 μmol/L concentration of compound **37** at denaturation temperatures ranging from 37 to 72 °C. (b) Cellular stabilization of DOT1L^{WT/R231Q} with different concentrations of compound **37** in the presence of Pronase E.

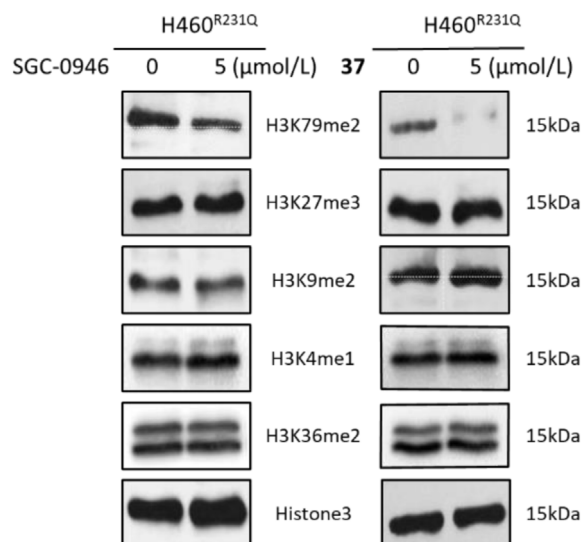


Figure 7 WB analysis of the effect of **37** on levels of common histone H3 modifications in H460^{R231Q} cells, with SGC0946 as the positive control.

35, it was hypothesized that the length of seven carbon units was beneficial. Additionally, the replacement of 4-hydroxypiperidino (**28**) with 4-ethylpiperazinyl (**29**) or morpholino (**30**) led to a decrease in potency, while the introduction of excessively long substituents (**31** and **32**) abolished the inhibitory effect on H460^{R231Q} cells.

Encouraged by the favorable efficacy of **28** and **35**, the following-up optimization of N-substituents focused on the γ -carbamoyl group with unclear effect, offering derivatives **36–42** with γ -tertiary amine (Table 5). Encouragingly, analog **36** strongly inhibited the proliferation of H460^{R231Q} cells within single digit

micromolar range, while **37** was identified as the most potent inhibitor with an IC₅₀ value of 6.18 μ mol/L, about 6-fold more potent than SGC0946. Both of them significantly reduced the H3K79me2 level mediated by DOT1L^{R231Q} at 5 μ mol/L (Fig. 5). Moreover, replacing the morpholino (**37**) with the 4-ethylpiperazinyl (**39**) disappointingly caused a 4-fold decreased activity against H460^{R231Q} cells. N-substituents without a terminally polar atom (**38** and **42**) were intolerant, neither did N-substituents with a terminally bulky group (**40** and **41**).

2.2. *In vitro* histone methyltransferase assay

Due to its excellent activity in cell assay, compound **37** was selected to detect the *in vitro* inhibitory effect against DOT1L^{R231Q}. Regrettably, the attempt to separate and purify the R231Q mutant protein of DOT1L failed, leading to the use of wild-type DOT1L instead. Unsurprisingly, **37** exhibited remarkably weaker inhibitory activity of DOT1L^{WT} (IC₅₀ = 2.08 μ mol/L) than SGC0946 (IC₅₀ = 18.36 nmol/L), primarily attributing to its bulky N-substituent (Supporting Information Fig. S1). Previous study demonstrated that a N-substituent slightly larger than isopropyl group would cause a significant drop of DOT1L^{WT} activity to micromolar level²⁷, which was consistent with enzymatic activity of **37**. On the other hand, bulky N-substituent presumably improved the selectivity for R231Q mutant protein.

2.3. Profiling of compound **37** in cell-based assays

The absence of DOT1L^{R231Q} enzymatic activity of compound **37** in histone methyltransferase assay prompted us to establish a cellular thermal shift assay (CETSA) to investigate cell permeability and cellular target engagement. As shown in Fig. 6a, compound **37** induced strong stabilization of DOT1L^{WT/R231Q} at denaturation temperatures ranging from 37 to 72 °C compared to DMSO control, especially ranging from 52 to 62 °C, confirming

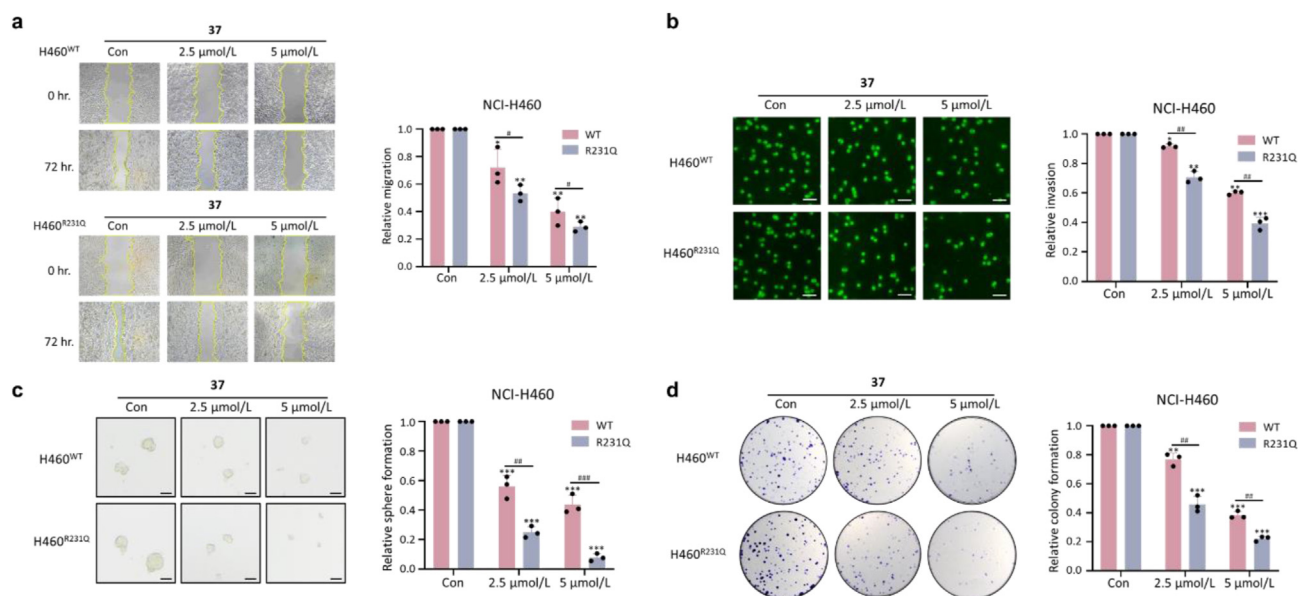


Figure 8 (a, b) Effect of **37** on cell migration and invasion in H460^{WT/R231Q} cells assessed by wound-healing assay (a) and Transwell assay (b), yellow lines demonstrate wound edges. (c, d) Effect of **37** on self-renewal and cell proliferation in H460^{WT/R231Q} cells assayed by tumorsphere formation analysis (c) and colony formation analysis (d) 7–14 days after seeding. Scale bars, 1000 μ m. Representative images and quantitative results are shown. Data are shown as means \pm SEM ($n = 3$). * $P < 0.05$, ** $P < 0.01$, and *** $P < 0.001$, as compared to the control group. # $P < 0.05$, ## $P < 0.01$, and ### $P < 0.001$, as compared to the WT group.

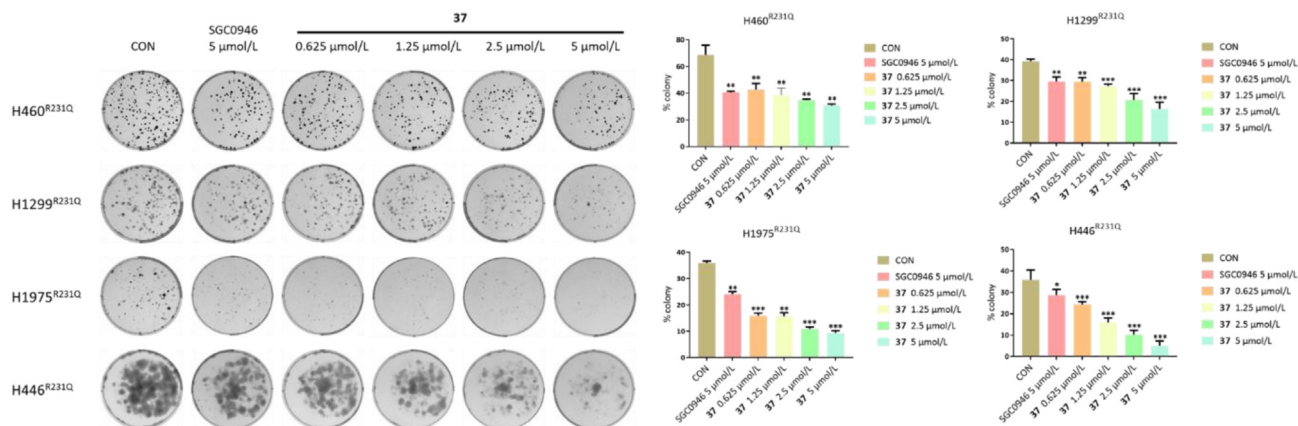


Figure 9 Compound **37** inhibited colony formation in H460^{R231Q}, H1299^{R231Q}, H1975^{R231Q}, and H446^{R231Q} lung cancer cells, with SGC0946 as the positive control. Quantification of the effect of **37** on colony formation expressed as % colony growth at different concentrations. The number of colonies was assessed by crystal violet staining 7–10 days after seeding. Data are shown as mean \pm SEM ($n = 3$). * $P < 0.05$, ** $P < 0.01$, *** $P < 0.001$.

the binding of **37** to the DOT1L^{WT/R231Q} proteins in the cellular system. To further investigate the interaction between **37** and DOT1L in cells, a drug affinity responsive target stability (DARTS) assay was performed (Fig. 6b). Similarly, treatment of H460^{WT/R231Q} cells with different concentrations of compound **37** effectively reduced the sensitivity of DOT1L^{WT/R231Q} to Pronase E, illustrating that **37** bound to and stabilized DOT1L^{WT/R231Q}. Noteworthy, compared with DOT1L^{WT}, **37** was identified with better

selectivity and stronger stabilization for R231Q mutant protein in both CETSA and DARTS assays. Owing to the wild-type DOT1L plays important roles in maintaining normal physiology, the favorable selectivity for R231Q mutant protein would be beneficial to reduce potential toxicity caused by DOT1L inhibitors.

In addition to DOT1L, several methyltransferases were also identified to be overexpressed in lung cancer cell lines, such as H3K9^{28,29} and H3K27^{30,31} methyltransferases. To identify that

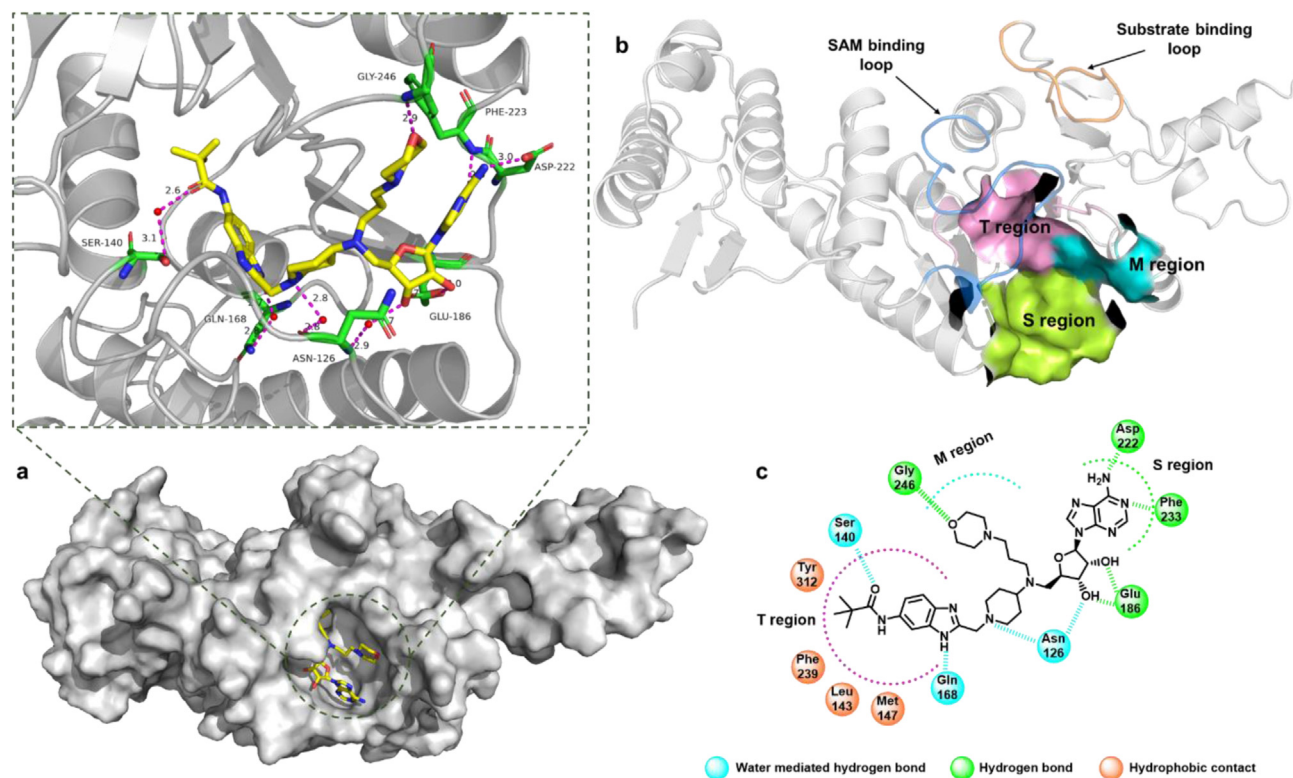


Figure 10 (a) Overview of the predicted complex of **37** (yellow sticks) and DOT1L^{R231Q} (gray) extracted from molecular dynamic simulation. A detailed view of the key residues (green sticks) is shown in the expanded view. Water molecules are displayed as red balls and hydrogen bonds are depicted as magenta dashed lines. (b) "Induced-fit" allosteric model, the S region is colored green, the M region is colored cyan, and the T region is colored pink. (c) Two-dimensional diagram of key interactions between **37** and DOT1L^{R231Q}.

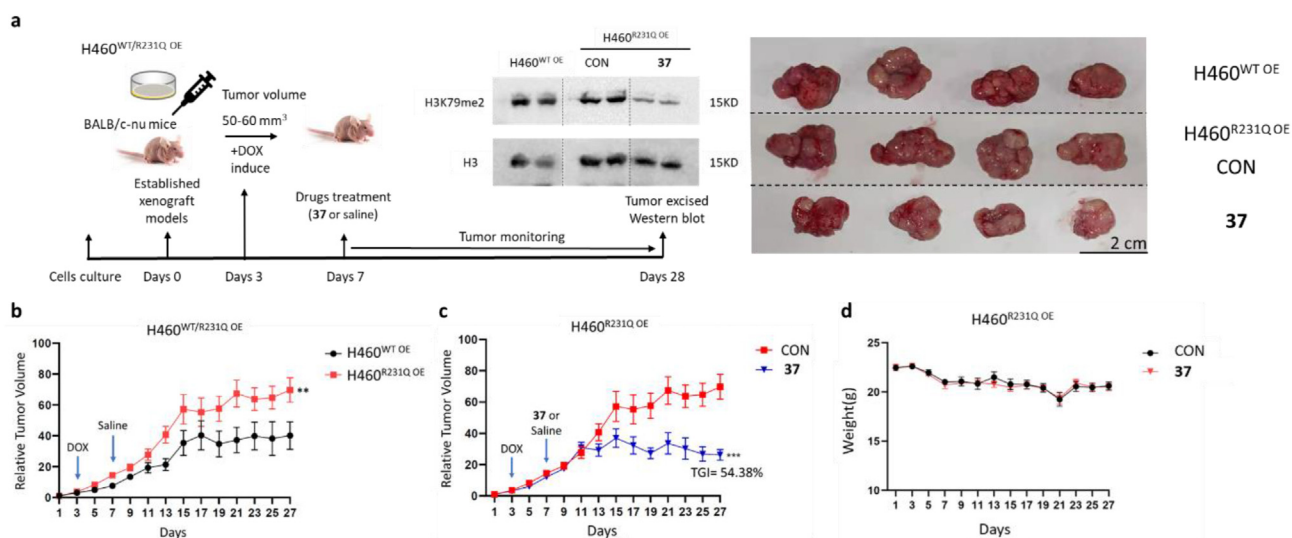


Figure 11 *In vivo* antitumor activity of compound **37** in the H460^{R231Q OE} CDX model. (a) The construction process of the H460^{WT/R231Q OE} CDX model, immunoblotting to detect the expression of H3K79me2 in tumor tissues and images of H460^{WT/R231Q OE} tumors from the mice ($n = 4$). (b) Tumor growth curves of the H460^{WT/R231Q OE} CDX model, intraperitoneal administration with saline (10% DMSO + 40% PEG300 + 5% Tween 80 + 45% saline, five times per week) (c) Tumor growth curves of the H460^{R231Q OE} CDX model, intraperitoneal administration with saline or **37** (20 mg/kg, five times per week). (d) Body weight changes of the mice. * $P < 0.05$, ** $P < 0.01$, *** $P < 0.001$.

compound **37** manifested its anti-proliferative activity against the H460^{R231Q} cell through DOT1L^{R231Q} inhibition, WB analysis of common histone H3 modifications was determined (Fig. 7). Treatment with both SGC0946 and **37** resulted in a decrease in H3K79me2 level, while H3K27me3, H3K9me2, H3K4me1 and H3K36me2 levels remained relatively unchanged, indicating favorable selectivity for DOT1L^{R231Q}. Besides, **37** corroborated a stronger ability to decrease the expression level of H3K79me2, which was consistent with the previous data.

Since the R231Q mutation comprehensively enhanced the proliferation, self-renewal, migration, and invasion abilities of lung cancer cells, a panel of *in vitro* assays was performed to verify the efficacy of **37** against H460^{WT} and H460^{R231Q} cells. Firstly, the anti-migration and anti-invasion effects of **37** were detected through the wounding-healing and transwell assays. As illustrated in Fig. 8a and b, treatment with **37** significantly reduced the number of migrating and invading cells at concentrations of

2.5 and 5 $\mu\text{mol/L}$, especially in the H460^{R231Q} cell group. In addition to cell migration, the inhibition of **37** on the self-renewal capacity of H460^{WT/R231Q} cells was investigated by the tumor-sphere formation assay. As shown in Fig. 8c, compound **37** prominently decreased the number and size of tumorspheres at 5 $\mu\text{mol/L}$, the efficiency of tumorsphere formation in H460^{WT} and H460^{R231Q} cells decreased by 56.4% and 92.1%, respectively. Similar results were also obtained in the colony formation assay, the number of colony formations in H460^{WT} and H460^{R231Q} cells decreased by 61.6% and 77.8% after the treatment of **37** at a dose of 5 $\mu\text{mol/L}$, respectively (Fig. 8d). Visually, photographs of selected colonies clearly indicated a more potent antigrowth effect of compound **37** on the H460^{R231Q} cell than the H460^{WT} cell. Altogether, these data suggested that **37** possessed outstanding

Table 6 Pharmacokinetic profiles of **37** *in vivo*.

Parameter	Compound 37	
	20 mg/kg (i.v.)	20 mg/kg (i.p.)
T_{max} (h)	0.083	0.19 \pm 0.10
C_{max} (ng/mL)	5842 \pm 456.8	2029 \pm 814.6
AUC_{0-t} (h·ng/mL)	2689 \pm 620	2651 \pm 567
$\text{AUC}_{0-\infty}$ (h·ng/mL)	2815 \pm 649	2735 \pm 657
$t_{1/2}$ (h)	1.62 \pm 1.35	1.93 \pm 0.91
CL (mL/kg/min)	122.94 \pm 29.61	
V_{ss} (L/kg)	7.59 \pm 4.71	
$\text{MRT}_{0-\infty}$ (h)	1.14 \pm 0.76	1.75 \pm 0.61
F (%)		97.2%

Five SD rats were used for each group. Data are averages of five independent determinations and reported as the mean \pm standard deviation (SD).

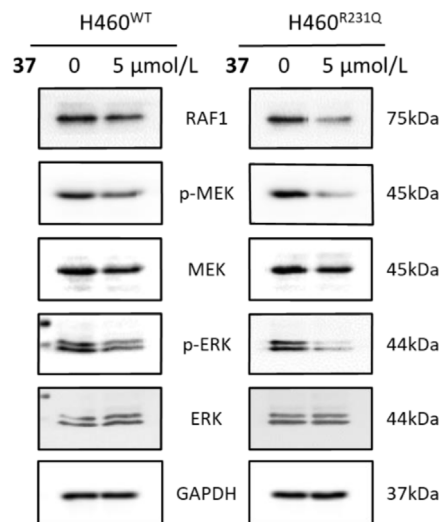


Figure 12 WB analysis of RAF1, p-MEK, MEK, p-ERK, and ERK expression levels in H460^{WT} and H460^{R231Q} cells.

inhibition on various malignant phenotypes of lung cancer cell lines carrying R231Q mutation along with high selectivity for DOT1L^{R231Q}.

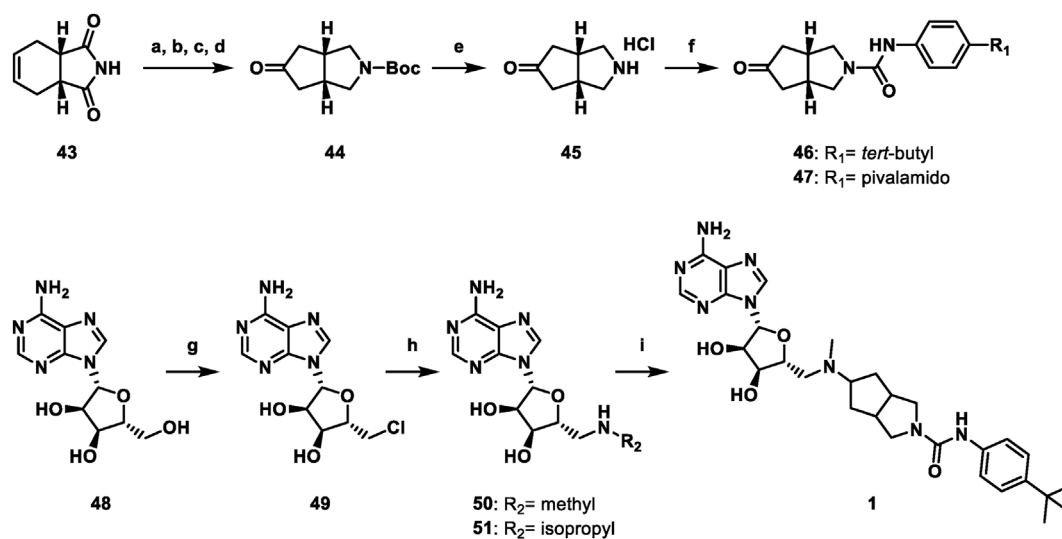
Despite favorable antiproliferation of **37** against the H460^{R231Q} cell, it was insufficient to assess **37** based on only one lung cancer cell line in colony formation assay. According to the expression level of endogenous DOT1L in cells (Supporting Information Fig. S2), three additional lung cancer cell lines were selected apart from low expressed H460 cells, including moderately expressed H1299 and H1975 cells and highly expressed H446 cells. Utilizing lentiviral transduction, H1299^{R231Q}, H1975^{R231Q}, and H446^{R231Q} cells expressing exogenous DOT1L^{R231Q} were established in a similar way to the H460^{R231Q} cell and used in colony formation assays. As shown in Fig. 9, the colony formation of four cell lines was effectively blocked by **37** in a progressive and remarkable manner. Furthermore, **37** exhibited better efficacy than SGC0946 at the same concentration. Indeed, treatment with compound **37** at 0.625 $\mu\text{mol/L}$ achieved fewer colonies than that of SGC0946 at 5 $\mu\text{mol/L}$ in both H1975 and H446 cells, while remarkable colony growth arrest was observed after administration at 5 $\mu\text{mol/L}$ dose of **37**.

2.4. Molecular dynamic simulation and “induced-fit” allosteric model

To investigate the binding mode of compound **37** with DOT1L^{R231Q} protein, a 100 ns molecular dynamic simulation was performed on the crystal structure of DOT1L^{WT} (PDB ID: 4ER6) whose residue Arg231 was mutated to Gln. The final conformation showed that the adenosine head of **37** occupied the SAM binding site and formed four pairs of hydrogen bonds with residues Asp222, Phe223, and Glu186 as expected (Fig. 10a). The benzimidazole tail entered the hydrophobic cavity in a similar manner to SGC0946 and formed multiple hydrophobic contacts. Moreover, the nitrogen atoms on benzimidazole and piperidine ring engaged in water-mediated hydrogen bonds with residues Asn126 and Gln168, respectively. Meanwhile, the oxygen atom of the

pivalamide moiety was able to establish an additional hydrogen bond through a water bridge with residue Ser140. Unexpectedly, the central N-side chain was located in an unrecognized region adjacent to the SAM binding site and formed a hydrogen bond with residue Gly246.

Interestingly, the protein–ligand root mean square deviation (RMSD) values once reached 4 Å during the whole simulation process (Supporting Information Fig. S3), and the measured RMSD values larger than 3 Å indicated a large conformational change of DOT1L^{R231Q} protein during the simulation. Also, the wild-type DOT1L is featured by its flexible SAM and substrate binding loops which enable DOT1L to accommodate different inhibitors through allosteric regulation³². Adenosine inhibitors, such as SGC0946 and EPZ004777, could induce the formation of the internal hydrophobic cavity by their bulky hydrophobic tails^{21,33}. Non-adenosine inhibitors developed by Novartis similarly induced conformational shifts within DOT1L, thereby creating an induced pocket in the vicinity of SAM binding site^{34,35,36}. Based on in-depth analysis of their cocrystal structures, it was discovered that the internal hydrophobic cavity and the induced pocket were located in the same region, surrounded by a cluster of hydrophobic residues Leu143, Val144, Met147, Val169, Phe239, Val267 and Tyr312 (Supporting Information Fig. S4). Resultantly, the “Induced-fit” allosteric model was proposed in the light of the binding modes of DOT1L^{WT} and DOT1L^{R231Q} inhibitors (Fig. 10b). According to the “Induced-fit” allosteric model, the inhibitors binding site within DOT1L can be divided into three regions, namely SAM binding site (S region), allosteric hydrophobic pocket (T region) and mutation-induced region (M region). The S region is a highly polar region originally designed for polar endogenous ligand, mainly accommodating the adenosine head and forming four pairs of vital hydrogen bonds. The T region is a flexible hydrophobic region that allosterically binds to the non-adenosine inhibitors or bulky hydrophobic tails of adenosine inhibitors. The M region is a special region formed by R231Q mutation, missense mutation of positively charged arginine to uncharged glutamine will break the original hydrogen



Scheme 1 Synthetic route of compound **1**. Reagents and conditions: (a) LiAlH₄, THF, 67 °C; (b) (Boc)₂O, THF, rt; (c) KMnO₄, TBAB, *n*-hexane, H₂O, 0 °C; (d) NaOAc, Ac₂O, 135 °C, 46% over four steps; (e) 4 N HCl/EtOAc, rt, 100%; (f) 4-*tert*-butylaniline, CDI, THF, rt, **46**; *N*-(4-aminophenyl)pivalamide, CDI, THF, rt, **47**; (g) SOCl₂, HMPA, rt, 95%; (h) CH₃NH₂ (40% aqueous), 80 °C, **50**; isopropylamine, 80 °C, **51**; (i) **46**, NaBH₃CN, MeOH, rt, 22%.

network (Supporting Information Fig. S5), resulting in increased flexibility of the local region. Furthermore, the flexible SAM binding loop is another critical structural basis of conformational rearrangement, both accounting for the enlarged SAM binding site and the formation of the M region. Therefore, the DOT1L^{WT} without the M region to accommodate a relatively bulky N-side chain was less sensitive to compound **37**.

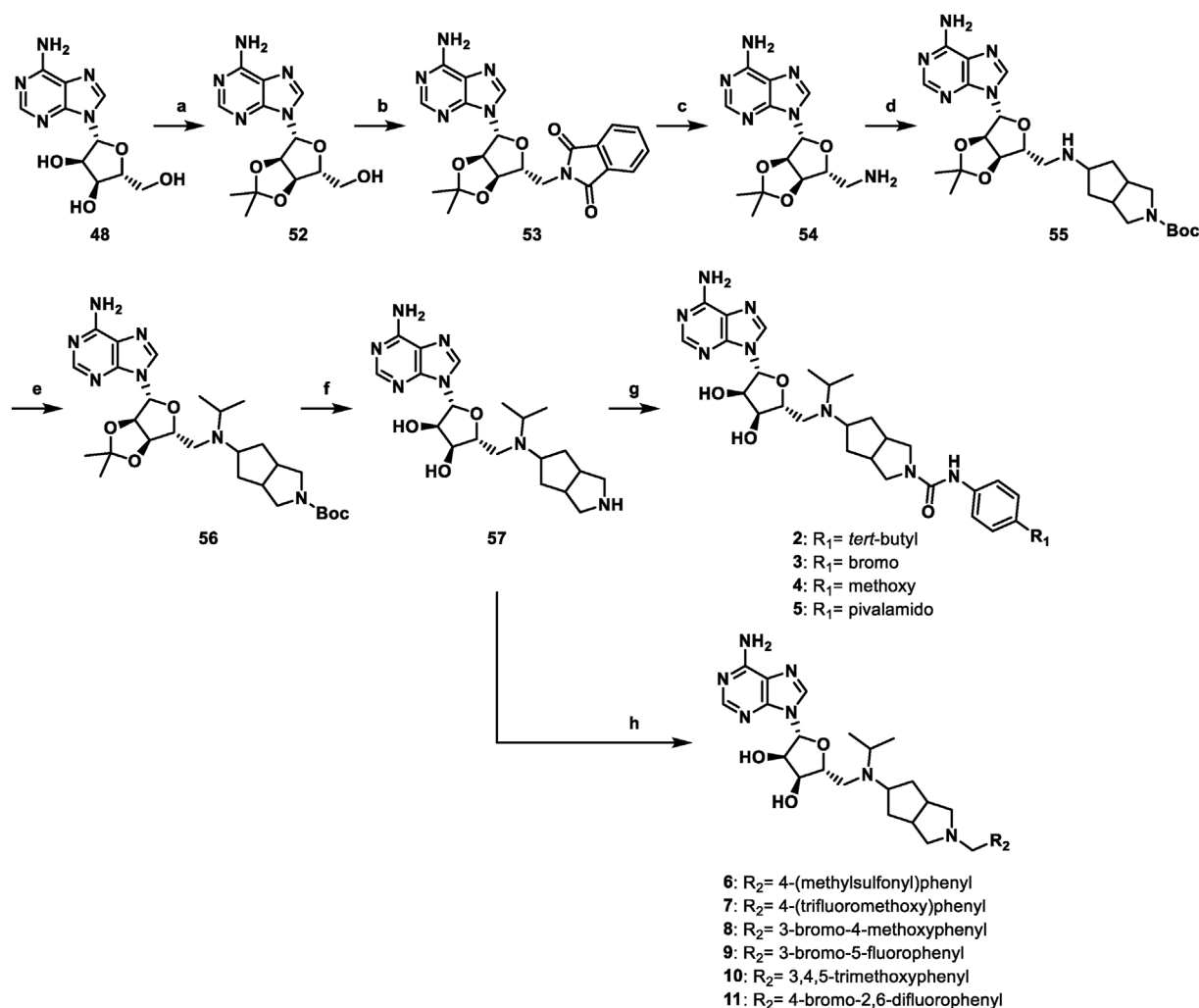
2.5. Antitumor activity *in vivo* of compound **37**

Considering the promising results obtained in cellular assays, the potential antitumor effect of compound **37** was investigated *in vivo*. To eliminate the effect of endogenous DOT1L on activity, we knocked down endogenous DOT1L in H460 cells and reintroduced DOT1L^{WT} or DOT1L^{R231Q} proteins *via* the Tet-on system, receiving H460^{WT/R231Q OE} cells. Male BALB/c-nu mice were subcutaneously inoculated with H460^{WT OE} or H460^{R231Q OE} cells respectively and divided into the H460^{WT OE} group and H460^{R231Q OE} group (Fig. 11a). Subsequently, the H460^{R231Q OE} group was randomly divided into control group (saline) and treatment group (compound **37**). As shown in Fig. 11b, no obvious

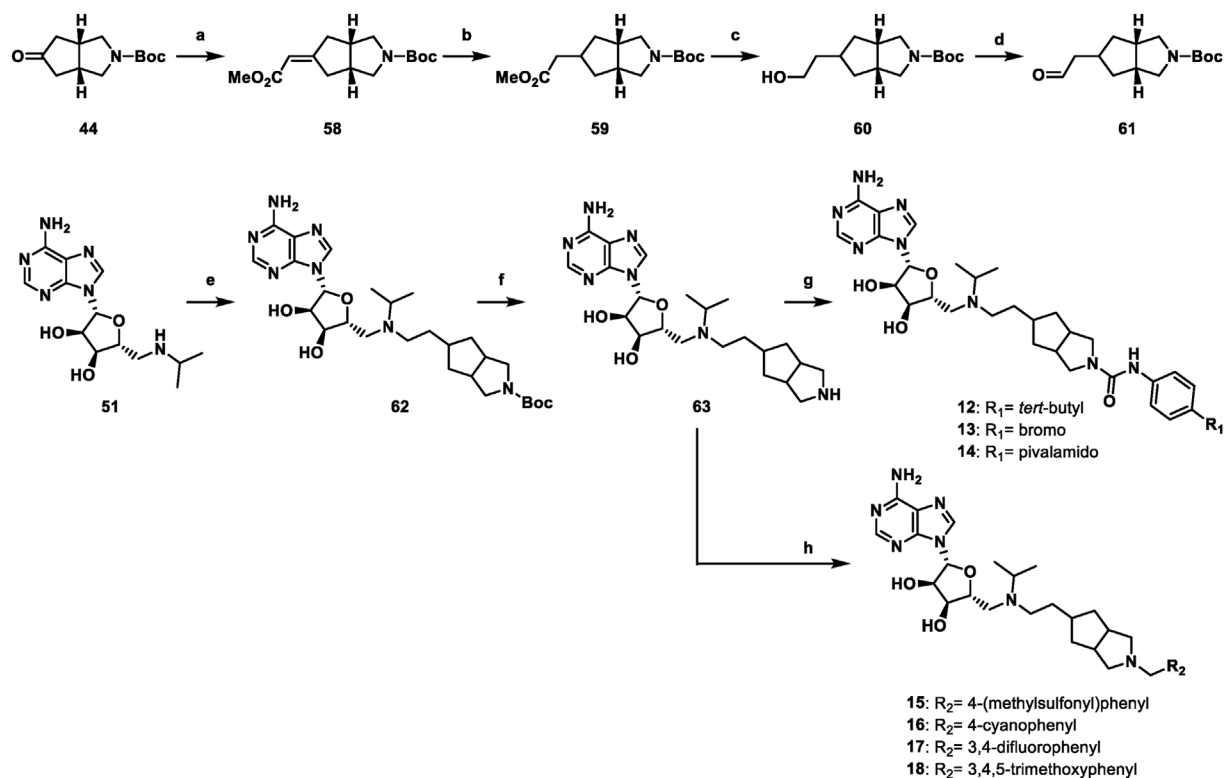
contrast was observed in tumor growth rate between the H460^{WT OE} group and the control group before doxycycline (DOX) induction on the third day. Since DOX induced the expression of exogenous DOT1L^{WT} and DOT1L^{R231Q}, both the H460^{WT OE} group and control group achieved greater tumor growth rate, and R231Q mutation was identified with stronger tumorigenicity *in vivo*. As shown in Fig. 11c, after intraperitoneal injection at 20 mg/kg dose for 3 weeks (five times per week), compound **37** displayed apparent antitumor efficacy with tumor growth inhibition (TGI) values of 54.38%. WB analysis of tumor tissue indicated higher expression of H3K79me2 in the control group than in the H460^{WT OE} group, which was significantly decreased after administration of **37** (Fig. 11a). In addition, the mice treated with **37** exhibited normal physical activity and body weight, demonstrating the good safety profile of **37** *in vivo* (Fig. 11d).

2.6. Pharmacokinetic profile of compound **37**

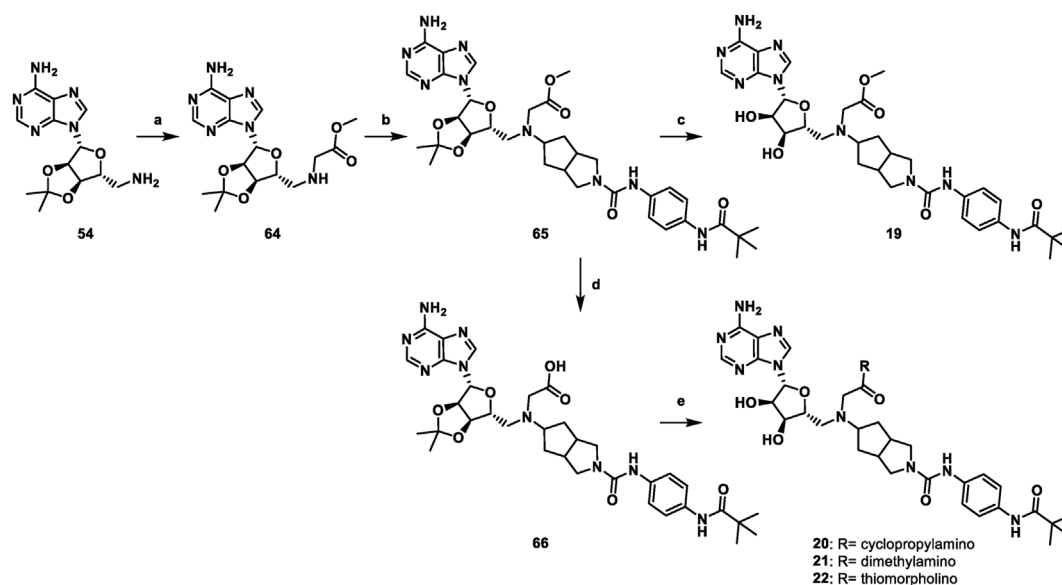
Aiming to investigate the pharmacokinetic profile of **37**, a pharmacokinetic study was performed *in vivo* and results were presented in Table 6. After intravenous (iv) and intraperitoneal (ip)



Scheme 2 Synthetic route of compounds **2–11**. Reagents and conditions: (a) PTSA, triethyl orthoformate, acetone, rt, 77%; (b) phthalimide, PPh₃, DIAD, THF, rt, 90%; (c) N₂H₄·H₂O, EtOH, 80 °C, 85%; (d) **44**, NaBH₃CN, MeOH, rt, 77%; (e) 2-iodopropane, K₂CO₃, ACN, 95 °C, 50%; (f) conc. HCl/THF, rt, 100%; (g) corresponding aniline, CDI, THF, rt, 28%–39%; (h) corresponding benzaldehyde, NaBH₃CN, MeOH, rt, 29%–35%.



Scheme 3 Synthetic route of compounds 12–18. Reagents and conditions: (a) NaH (60% dispersion in mineral oil), methyl diethylphosphonoacetate, THF, rt, 80%; (b) H₂, Pd/C, MeOH, rt, 100%; (c) LiAlH₄, THF, 0 °C, 96%; (d) Dess-Martin periodinane, NaHCO₃, CH₂Cl₂, rt, 90%; (e) **61**, NaBH₃CN, MeOH, rt, 44%; (f) TFA, CH₂Cl₂, rt, 76%; (g) corresponding aniline, CDI, THF, rt, 36%–56%; (h) corresponding benzaldehyde, NaBH₃CN, MeOH, rt, 28%–65%.



Scheme 4 Synthetic route of compounds 19–22. Reagents and conditions: (a) methyl bromoacetate, TEA, MeOH, 50 °C, 69%; (b) **47**, NaBH₃CN, MeOH, rt, 65%; (c) TFA, H₂O, rt, 83%; (d) 3 N NaOH solution, EtOH, 60 °C, 100%; (e) i) corresponding amine, EDCl, HOBT, TEA, CH₂Cl₂, rt; ii) conc. HCl, THF, rt, 41%–49% over two steps.

administration at a single dose (20 mg/kg), compound **37** exhibited a favorable area under the curve ($AUC_{0-t} = 2651 \pm 567$ h ng/mL), acceptable terminal half-life ($t_{1/2} = 1.93 \pm 0.91$ h) and excellent

intraperitoneal bioavailability ($F = 97.2\%$). Meanwhile, a high clearance was also observed with the value of 122.94 ± 29.61 mL/kg/min, partly attributing to the adenosine moiety of **37** which

could be recognized and metabolized by numerous enzymes³⁷. Likewise, as the only DOT1L inhibitor in clinical trials, EPZ5676 containing adenosine core also suffered from inferior pharmacokinetic profile, such as high clearance (68 mL/kg/min) and low oral bioavailability ($F = 0\%$)³⁸.

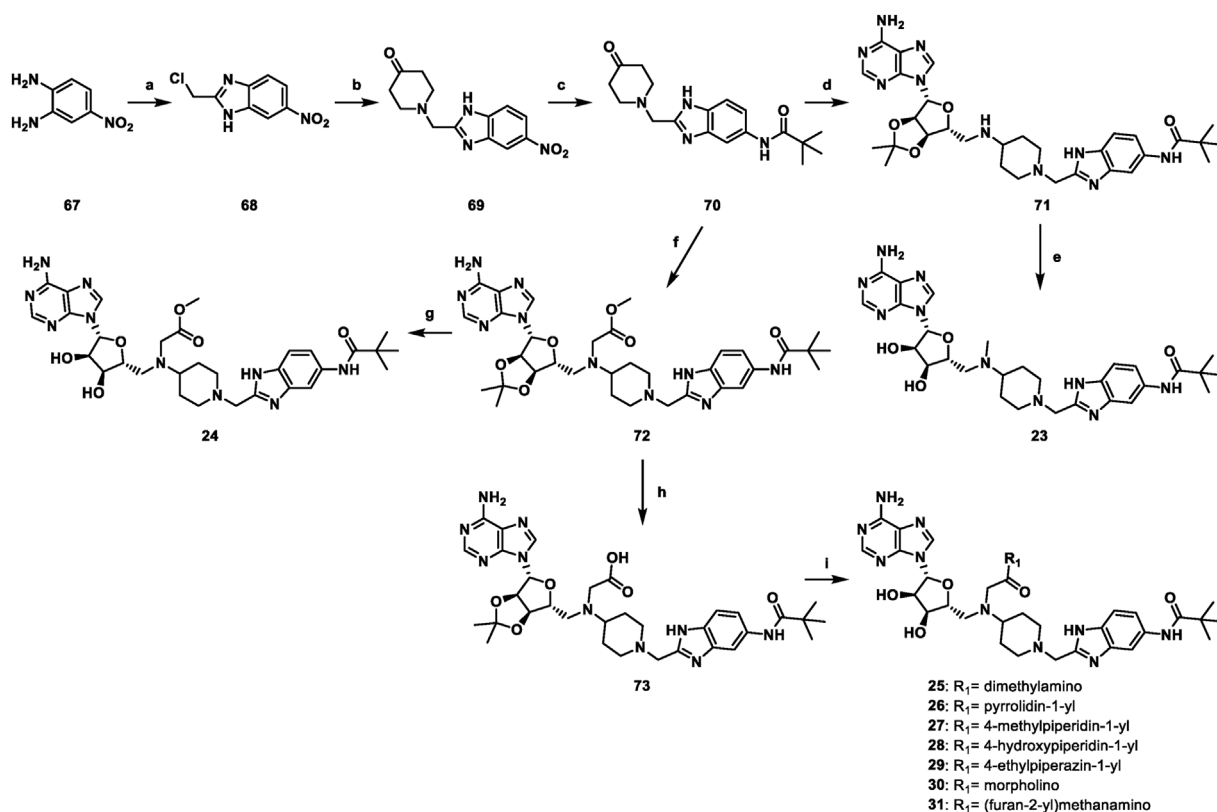
2.7. Effect of compound 37 on MAPK signaling pathway

Mechanistically, DOT1L^{R231Q} featured by higher enzymatic activity would raise the level of H3K79me2 in cancer cells, which in turn accumulated at the *RAF1* promoter as well as the promoter regions of *ELK3* and *KLF4* functioned downstream of MAPK. The enriched H3K79me2 at the *RAF1* promoter favored an active chromatin state to increase *RAF1* expression and promote the MAPK signaling cascades, eventually strengthening the malignancy of lung cancer (Fig. 1)¹⁹. To investigate the effect of 37 on the MAPK signaling pathway in H460^{WT} and H460^{R231Q} cells, WB assay was used to detect the expression of *RAF1* and the phosphorylation levels of MEK and ERK after treatment with 37 at a concentration of 5 $\mu\text{mol/L}$. As shown in Fig. 12, compound 37 markedly decreased the expression of *RAF1*, p-MEK, and p-ERK in the H460^{R231Q} cell. By contrast, the H460^{WT} cell was less inhibited by 37, with only a slight decrease of *RAF1*, p-MEK, and p-ERK levels. In conclusion, these results suggested that 37 inhibited the malignant phenotypes of lung cancer cells harboring DOT1L gain-of-function mutations via the MAPK/ERK signaling pathway.

2.8. Chemistry

The synthetic strategy furnishing compound 1 is depicted in Scheme 1. Utilizing commercially available *cis*-1,2,3,6-tetrahydrophthalimide (43) as starting material, intermediate 44 was prepared through the four steps previously reported³⁹, namely LiAlH_4 mediated reduction, Boc protection, KMnO_4 mediated oxidation and Dieckmann condensation. Subsequently, Boc deprotection (45) followed by CDI-mediated condensation with 4-*tert*-butylaniline or *N*-(4-aminophenyl)pivalamide afforded intermediates 46 and 47, respectively. Starting from commercially available adenosine (48), treatment with thionyl chloride gave intermediate 49. Then 49 reacted with 40% methylamine solution or isopropylamine in seal tubes to afford 50 and 51, respectively. Compound 1 was obtained by reductive amination of 50 with ketone 46 in the presence of sodium cyanoborohydride.

The synthesis of compounds 2–11 is described in Scheme 2. Due to the large steric hindrance caused by the isopropyl group, 51 could not react with ketone 46 to prepare compound 2 directly, resulting in the development of a new synthetic route. The 2',3'-ribose diol of 48 was ketal protected using acetone to furnish 52, followed by conversion of hydroxyl group (52) to primary amine (54) by Gabriel Synthesis. Reductive amination of 54 with ketone 44 gave intermediate 55 in 77% yield, which was reacted with 2-iodopropane at 90 °C in a sealed tube to obtain 56. Then,



Scheme 5 Synthetic route of compounds 23–31. Reagents and conditions: (a) chloroacetic acid, conc. HCl solution, H₂O, 110 °C, 86%; (b) 4-piperidone hydrochloride monohydrate, K₂CO₃, THF, 65 °C, 87%; (c) i) Raney Ni, H₂, MeOH, rt; ii) pivaloyl chloride, TEA, *i*PrOH, rt, 47%; (d) 54, NaBH₃CN, MeOH, rt, 79%; (e) i) formaldehyde, NaBH₃CN, MeOH, rt; ii) conc. HCl, THF, rt, 32%; (f) 64, NaBH₃CN, MeOH, rt, 70%; (g) conc. HCl, THF, rt, 59%; (h) 3 N NaOH solution, EtOH, 60 °C, 100%; (i) i) corresponding amine, EDCI, HOBT, TEA, CH₂Cl₂, rt; ii) conc. HCl, THF, rt, 18%–41%.

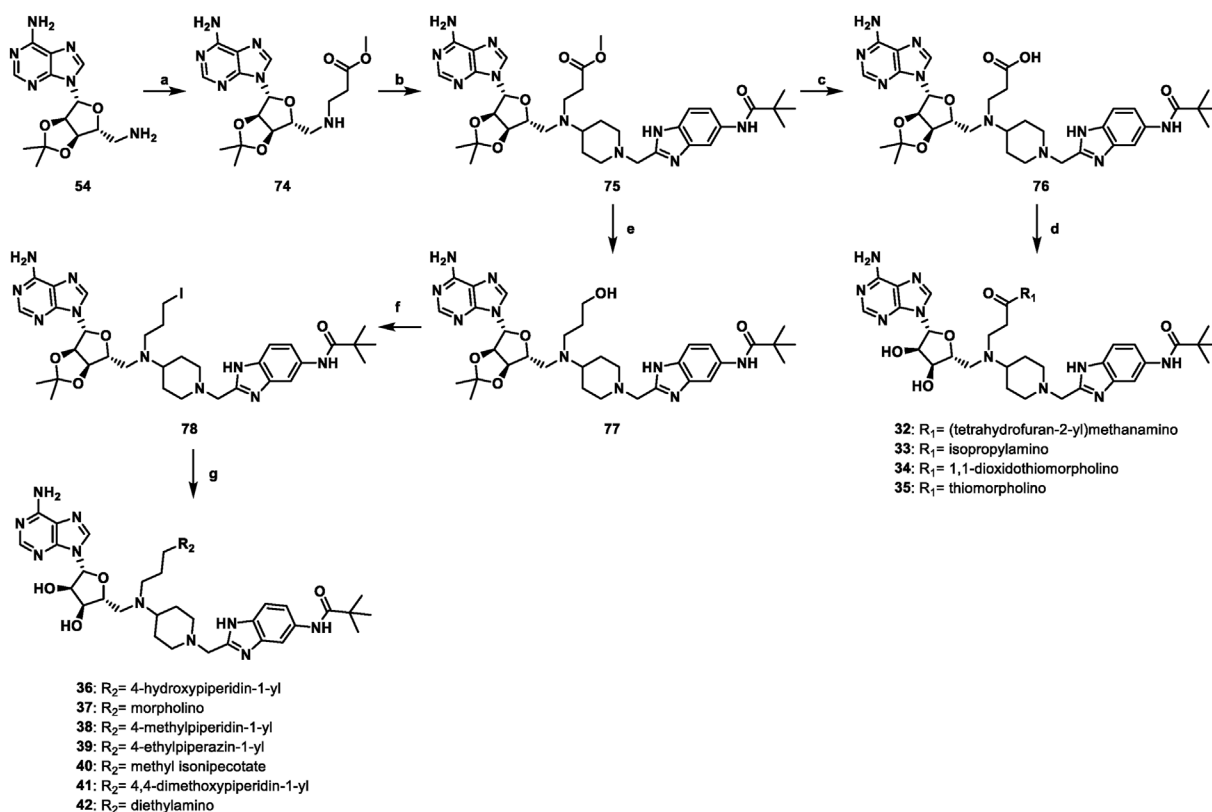
simultaneous removal of ketal and Boc protect groups under acidic conditions provided **57**, which served as a flexible intermediate for CDI-mediated condensation with various anilines or reductive amination with various benzaldehydes provided compounds **2–5** and **6–11**, respectively.

The synthesis of compounds **12–18** is described in Scheme 3. The Horner-Wadsworth-Emmons reaction of **44** with methyl diethylphosphonoacetate furnished **58**, which was hydrogenated over palladium on carbon at room temperature to afford **59**. Reduction of the ester group using LiAlH₄ gave alcohol **60**, followed by Dess-Martin oxidation to produce aldehyde **61** in excellent yield. Then, **61** reacted with intermediate **51** via reductive amination to give **62**, which was subjected to Boc deprotection under trifluoroacetic acid (TFA) conditions to yield **63**. Compounds **12–18** were prepared from **63** in the same manner as described for **2–11**.

The synthetic pathway of compounds **19–22** is outlined in Scheme 4. Intermediate **64** was prepared from **54** via nucleophilic substitution reaction with methyl bromoacetate under basic conditions, followed by reductive amination with **47** to provide intermediate **65**, which finally yielded compound **19** by removing the ketal protecting group. Additionally, **65** was hydrolyzed in the presence of 3 N NaOH solution to obtain **66**, which was subjected to condensation with various amines using EDCI and HOBt as coupling reagents and subsequent ketal deprotection under hydrochloric acid conditions to afford compounds **20–22**.

The synthesis of compounds **23–31** is described in Scheme 5. Using commercially available 4-nitro-*o*-phenylenediamine (**67**) as starting material, **68** was obtained by cyclization reaction with the chloroacetic acid in hydrochloric acid. Nucleophilic substitution of **68** with 4-piperidone hydrochloride monohydrate gave **69**. The nitro group of **69** was reduced using hydrogen and Raney Ni and then acylated with pivaloyl chloride to furnish **70**, which was subjected to reductive amination with **54** to deliver **71** in good yield. Compound **23** was prepared from **71** by introducing a methyl group via reductive amination with formaldehyde and removing the ketal protecting group under hydrochloric acid conditions. Similarly, compound **24** was prepared from **70** by reductive amination with **64** and ketal deprotection. Compounds **25–31** were prepared from **72** in the same manner as described for **20–22**, namely hydrolysis of ester, condensation with various amines in the presence of EDCI and HOBt, and deprotection of the ketal group.

The synthesis of compounds **32–42** is described in Scheme 6. A Michael addition of **54** with methyl acrylate gave intermediate **74**, followed by reductive amination with **70** to afford intermediate **75**. Compounds **32–35** were prepared from **75** in the same manner as described for **20–22**. Alternatively, the ester group of **75** was reduced by LiAlH₄ to alcohol **77**, which was subjected to an iodination reaction in the presence of imidazole and PPh₃ to give **78**. Nucleophilic substitution of **78** with various amines and removal of the ketal protecting group finally delivered compounds **36–42** in different yields.



Scheme 6 Synthetic route of compounds **32–42**. Reagents and conditions: (a) methyl acrylate, MeOH, 60 °C, 76%; (b) **70**, NaBH₃CN, MeOH, rt, 83%; (c) 3 N NaOH solution, EtOH, 60 °C, 100%; (d) i) corresponding amine, EDCI, HOBt, TEA, CH₂Cl₂, rt; ii) conc. HCl, THF, rt, 22%–33%; (e) LiAlH₄, THF, rt, 72%; (f) I₂, PPh₃, imidazole, THF, rt, 74%; (g) i) corresponding amine, K₂CO₃, ACN, 45 °C; ii) conc. HCl, THF, rt, 17%–52%.

3. Conclusions

Given the oncogenic role of DOT1L and its mutations in lung cancer, corresponding inhibitors would be highly beneficial for the treatment of lung cancer. However, the discovery of drugs targeting DOT1L has been quite challenging, with no candidate approved for marketing to date. Moreover, multiple gain-of-function mutations represented by R231Q dramatically enhanced the malignant phenotypes of lung cancer cells, while none of potent DOT1L^{R231Q} inhibitors has been disclosed.

In this work, utilizing SGC0946 as a lead, the first series of DOT1L^{R231Q} inhibitors were discovered by incorporating hexahydrocyclopenta[c]pyrrole linker to fill the enlarged cavity within the mutant protein. Although several compounds displayed comparable potency to SGC0946 in antiproliferation and WB assays, the excessive rigidity of bulky bicyclic linker impeded the improvement of activity, thereby driving the structural optimization on hexahydrocyclopenta[c]pyrrole-2(1*H*)-carboxamide fragment. Accordingly, the second series of DOT1L^{R231Q} inhibitors bearing relatively flexible piperidine linker and hydrophobic benzimidazole tail were designed. Through antiproliferation assay in the H460^{R231Q} cell, **37** was identified as the most potent inhibitor with an IC₅₀ value of 6.18 μmol/L, about 6-fold more potent than SGC0946. Subsequently, CETSA and DARTS assays validated the cell permeability and cellular target engagement of **37**, while WB analysis of common histone H3 modifications in the H460^{R231Q} cell confirmed the favorable selectivity of **37** for DOT1L^{R231Q}. Meanwhile, **37** effectively inhibited the migration, invasion, self-renewal, and colony formation in lung cancer cell lines overexpressed DOT1L^{R231Q}. In addition to sharing a similar binding mode with SGC0946, the molecular dynamic simulation indicated that **37** formed an additional hydrogen bond with the residue Gly246, accounting for improved DOT1L^{R231Q} activity. Moreover, based on the binding modes of **37** and reported DOT1L^{WT} inhibitors with DOT1L^{R231Q/WT}, the “Induced-fit” allosteric model was first proposed to facilitate the development of potent inhibitors targeting DOT1L and its mutations.

To further assess the antitumor activity of **37**, the H460^{R231Q} OE CDX models in mice were established by excluding the influence of endogenous DOT1L *via* gene knockdown. *In vivo* study demonstrated **37** significantly inhibited tumor growth at a dose of 20 mg/kg, achieving 54.38% TGI without obvious toxicity. Furthermore, **37** exhibited good pharmacokinetic properties with an acceptable half-life ($t_{1/2} = 1.93 \pm 0.91$ h) and excellent bioavailability ($F = 97.2\%$) after intraperitoneal administration. In the mechanism study, **37** decreased RAF1 expression and inhibited the phosphorylation of MEK and ERK, validating that **37** exerted anticancer activity by regulating the MAPK/ERK pathway. Overall, **37** provided a chemical tool for better defining the biological roles and the therapeutic potential of DOT1L^{R231Q} and a valuable design idea for the development of optimized derivatives targeting DOT1L^{R231Q} with increased potency.

4. Experimental

4.1. Chemistry

The synthetic procedures and characterization data of all intermediates and target compounds were described in [Supporting Information](#).

4.2. Cell-based assays

Three human NSCLC cell lines (NCI-H460, NCI-H1299, NCI-H1975) and one human SCLC cell line (NCI-H446) were obtained from the American Type Culture Collection and were cultured in RPMI 1640 medium (Gibco), with 10% fetal bovine serum (Gibco) and 1% penicillin-streptomycin (Gibco) at 37 °C in a humidified incubator with 5% CO₂. Lung cancer cell lines (H460^{WT/R231Q}, H460^{WT/R231Q} OE, H1299^{R231Q}, H1975^{R231Q}, H446^{R231Q}) ectopically expressing wild-type or R231Q mutant DOT1L proteins (aa 1–416) were constructed according to the methods reported by our research group¹⁹.

4.2.1. Cell proliferation assay

Cells were inoculated in 96-well plates at an appropriate density and incubated with various concentrations of agents for 72 h at 37 °C in a 5% CO₂ incubator. Cell Counting Kit-8 (MCE) and multi-mode plate reader (Molecular Devices) were used according to the manufacturer's instructions to measure cell growth.

4.2.2. Western blot analysis

Cells were collected and lysed in RIPA buffer (Cell Signaling Technology) containing 1% Protease Inhibitor Cocktail (MCE) and 1% Phosphatase Inhibitor Cocktail (MCE) or EpiQuik™ Total Histone Extraction Kit (EpiGentek), and protein concentration was determined using the BCA Protein Assay Kit (Thermo Fisher Scientific). Protein extracts were separated on 8%–15% SDS-PAGE by electrophoresis and transfer equipment (Bio-Rad) and transferred to PVDF membranes (Millipore). The PVDF membrane was blocked and incubated with the corresponding primary and secondary antibodies, reacted with ECL detection reagent (PerkinElmer) and exposed to X-ray films. For the detection of proteins with the same or similar molecular weight, stripping the primary antibody with ReBlot Plus Strong Antibody Stripping Solution (Millipore), and re-incubating the corresponding primary and secondary antibodies for chemiluminescence. Protein bands were quantified using Image J software, and the relative H3K79me2 levels were calculated by normalizing raw H3K79me2 measurements to histone H3 signals.

4.2.3. Cellular thermal shift assay (CETSA)

Cells were incubated with or without compound **37** for 7 days, and then cells were precipitated directly by centrifugation and made into cell lysis. and then, each lysate was equally divided into 8 parts, each part was heated for 3 min under different temperatures (37, 42, 47, 52, 57, 62, 67, and 72 °C). The precipitated proteins were separated from the soluble fraction by centrifugation, and it was boiled at 95 °C for 10 min for WB analysis.

4.2.4. Drug affinity responsive target stabilization assay (DARTS)

Cells were incubated with or without compound **37** for 7 days, and then cells were precipitated directly by centrifugation and made into cell lysis. Cell lysis solution was treated with 10 μg/mL pronase E per sample for 10 min at room temperature. Samples were boiled immediately after adding loading buffer to stop the digestion and then analyzed by Western blot.

4.2.5. Wound healing assay

Cells at the logarithmic growth stage were seeded in 12-well plates for overnight culture. When the cells were adherent to the

wall in a single layer, a standard 10- μ L pipette tip was used to make a straight incision in the cell layer. The suspension cells were cleaned and removed with PBS (Gibco), and the incubation was continued for 72 h in a serum-free medium with different concentrations of compound **37**. Photographs were taken at 0 and 72 h under an inverted microscope (Nikon).

4.2.6. Transwell migration assay

Cells were starved for 12 h. The top surface of the membrane in the upper Transwell chamber was coated with Matrigel. Cells were diluted to 25×10^4 /mL with serum-free medium containing different concentrations of compound **37**, and 200 μ L cell suspension was added to the upper Transwell chamber, and 700 μ L medium containing 12% fetal bovine serum was added to the lower chamber. After incubation for 72 h, cells were fluorescently labeled with Calcein AM (Sigma–Aldrich). Finally, cell invasion was evaluated by an inverted microscopy (Nikon).

4.2.7. Tumorsphere formation assay

Cells were seeded into low-attachment surface six-well plates (Corning) with continuous culture in DMEM/F12 medium (Gibco), containing B27 supplement (Gibco), FGF (20 ng/mL), EGF (20 ng/mL) and different concentrations of compound **37** for 7–14 days. Photographs were taken under an inverted microscope (Nikon) and counted when the number of spheres with a diameter larger than 50 μ m.

4.2.8. Colony formation assay

Cells were seeded in 12-well plates and then treated in a complete medium with different concentrations of compound **37** for 7–14 days. The medium was renewed every 3 days. Cells were fixed using 100% methanol for 15 min and stained with 1% crystal violet for 30 min at room temperature. After air drying at room temperature, plates were photographed (Nikon) under light microscopy to count the number of colonies.

4.3. DOT1L^{WT} methyltransferase assay

DOT1L was purchased from Reaction Biology and the IC₅₀ values were determined by time-resolved Förster resonance energy transfer (TR-FRET) assay. Briefly, the 3 μ L/well of DOT1L Working solution and 5 nL/well of compound **37** or control (1% DMSO as vehicle control, SGC0946 as positive control) were mixed in a white 384-well plate (ProxiPlateTM-384 Plus, PerkinElmer) and incubated at 25 °C for 15 min. Then, 2 μ L/well of Nucleosomes & SAM Working solution was added and incubated at 25 °C for 60 min. Next, 1 μ L/well of Detection buffer was added and incubated at 25 °C for 10 min. Subsequently, 2 μ L/well of anti-SAH-Lumi4-Tb Working solution and 2 μ L/well of SAH-d2 Working solution were added and incubated at 25 °C for 60 min. Finally, the plate was read with an Envision 2105 (Ratio = $665 \text{ nm}/620 \text{ nm}$ as TR-FRET value, PerkinElmer). Inhibition (%) = $[1 - (\text{RLU}_{\text{cpd}} - \text{RLU}_{\text{positive}}) / (\text{RLU}_{\text{vehicle}} - \text{RLU}_{\text{positive}})] \times 100$, RLU is the TR-FRET value. The dose-response of inhibition test was carried out in duplicate and the IC₅₀ data was calculated using the software GraphPad Prism 8.

4.4. Molecular dynamic simulation

4.4.1. Molecular docking

A molecular docking study of compound **37** to DOT1L^{R231Q} was carried out with the software Schrödinger Glide. The DOT1L^{R231Q}

crystal structure was obtained based on DOT1L^{WT} (PDB code: 4ER6) whose residue Arg231 was mutated to Gln. Then, DOT1L^{R231Q} was processed by default with the Protein Preparation Wizard tool, and the prepared protein–ligand complex was defined as the binding site. The size of the docking grid box was 20 Å \times 20 Å \times 20 Å. Based on the OPLS_2005 force field, the grid of DOT1L^{R231Q} crystal structure was generated. The ligands were processed by default with the LigPrep tool, and the standard precision (SP) mode was set for docking studies without constrained binding to gain results.

4.4.2. Molecular dynamics simulation

The molecular dynamics simulations were used to study the binding mode given by molecular docking. Multiple stages were involved in Molecular dynamics: system building, simulation, and results analysis. The system was set in an orthorhombic box, which extended approximately 10 Å in each direction. The OPLS4 force field was used in the protein–ligand system. Subsequently, a minimization step was subjected to the system with the largest interaction setting of 2000 and the convergence threshold setting to 1.0 kcal/mol/Å using a hybrid method of the steepest decent and the limited-memory Broyden–Fletcher–Goldfarb–Shanno algorithms (LBFSGS). The system energy was reduced to the maximum of 5000 steps until it reached the gradient threshold of 25 kcal/mol/Å. The protein–ligand systems were minimized at a temperature of 300 K in the NPT ensemble using a Nose–Hover thermostat at 300 K and Martyna–TobiasKlein barostats at 1.01325 bar pressure. During the 100 ns simulation, the energy and the trajectory of the systems were calculated and recorded every 1.0 and 5.0 ps, respectively. The root mean square deviation (RMSD), protein–ligand interactions, and ligand torsion of rotatable bonds were analyzed.

4.5. In vivo xenograft model

In CDX studies, 2×10^6 H460^{WT/R231Q OE} cells suspended in PBS (Gibco) containing Matrigel (BD Biosciences) were inoculated subcutaneously into the right flank of 6–8-week-old male BALB/c-nu mice and visible tumors were measured with digital calipers. When the average tumor volume reached 50–60 mm³, the mice were randomly divided into the control group and the treatment group. The tumor size and body weight were measured every 2 days, and the tumor volume was calculated using the formula volume = $0.5 \times \text{length} \times \text{width}^2$. At the end of the experiment, the mice were sacrificed, and the tumors were stored at –80 °C or fixed in formalin for subsequent determination of tumor tissue protein expression. These experiments were performed in strict accordance with the recommendations in the Guide for the Care and Use of Laboratory Animals of the National Institutes of Health, and the corresponding protocols were approved by the Animal Experimentation Ethics Committee of Shenyang Pharmaceutical University.

4.6. Pharmacokinetic studies

Male SD rats were used in this study. The animals were randomly assigned to the treatment groups before the pharmacokinetic study, all animals were fasted for 12 h before dosing. Nine time points (0.083, 0.25, 0.5, 0.75, 1, 2, 4, 6 and 10 h for iv; 0.083, 0.25, 0.5, 0.75, 1, 2, 4, 6 and 10 h for ip) were set for this pharmacokinetic study. Each treatment group included 5 animals. There was also a control group of 2 animals. Blood collection was

performed from the orbital sinus in Microtainers containing heparin. All samples were immediately processed, flash-frozen, and stored at -70°C until subsequent analysis. Animals were sacrificed by cervical dislocation after the blood samples collection. The study design, treatment schedules for dosing, sample processing, sample analysis, LC-MS/MS conditions, preparation of calibration standards, and detailed analysis of the pharmacokinetic study results, including plasma concentration-time curves of compound **37**, are described in the [Supporting Information](#).

Acknowledgments

This work was supported by the National Natural Science Foundation of China (No. 82173685 and No. 82073320), Chinese Pharmaceutical Association-Yi ling Biomedical Innovation Fund (No. CPAYLJ202001, China), Liao Ning Revitalization Talents Program (No. XLYC2002115, China), Key R&D Plan of Liaoning Province in 2020 (No. 2020020215-JH2/103, China), Development Project of Ministry of Education Innovation Team (No. IRT1073, China), Natural Science Foundation of Shenyang (22-315-6-11, China).

Author contributions

Zehui Tan designed and synthesized compounds, performed the structure identification and DOT1L methyltransferase assay, and wrote the manuscript; Ning Guo, Jiayu Zhang and Wencai Lv completed the cell-based assays and *in vivo* study; Zhi Cao performed molecular dynamic simulation; Shuyu Liu conducted the synthesis of compounds; Linghe Zang, Deyi Ma and Jiahao Zhang conducted the pharmacokinetic studies; Nan Jiang analyzed and interpreted the data; Lihui Wang reviewed and edited the manuscript and provided funding acquisition; Xin Zhai conceived and directed the project conceptualization and project administration, wrote and revised the manuscript, and provided funding acquisition. All authors have given approval to the final version of the manuscript.

Conflicts of interest

The authors have no conflicts of interest to declare.

Appendix A. Supporting information

Supporting information to this article can be found online at <https://doi.org/10.1016/j.apsb.2024.03.018>.

References

- Zhu D, Zhang Y, Wang S. Histone citrullination: a new target for tumors. *Mol Cancer* 2021;**20**:90.
- Feng Q, Wang H, Ng HH, Erdjument-Bromage H, Tempst P, Struhl K, et al. Methylation of H3-lysine 79 is mediated by a new family of HMTases without a SET domain. *Curr Biol* 2002;**12**:1052–8.
- Krivtsov AV, Feng Z, Lemieux ME, Faber J, Vempati S, Sinha AU, et al. H3K79 methylation profiles define murine and human MLL-AF4 leukemias. *Cancer Cell* 2008;**14**:355–68.
- Bernt KM, Zhu N, Sinha AU, Vempati S, Faber J, Krivtsov AV, et al. MLLrearranged leukemia is dependent on aberrant H3K79 methylation by DOT1L. *Cancer Cell* 2011;**20**:66–78.
- Kurani H, Razavipour SF, Harikumar KB, Dunworth M, Ewald AJ, Nasir A, et al. DOT1L is a novel cancer stem cell target for triple-negative breast cancer. *Clin Cancer Res* 2022;**28**:1948–65.
- Nassa G, Salvati A, Tarallo R, Gigantino V, Alexandrova E, Memoli D, et al. Inhibition of histone methyltransferase DOT1L silences ER α gene and blocks proliferation of antiestrogen-resistant breast cancer cells. *Sci Adv* 2019;**5**:eaav5590.
- Annala M, Kivinummi K, Leinonen K, Tuominen J, Zhang W, Visakorpi T, et al. DOT1L-HES6 fusion drives androgen independent growth in prostate cancer. *EMBO Mol Med* 2014;**6**:1121–3.
- Vatapalli R, Sagar V, Rodriguez Y, Zhao JC, Unno K, Pamarthy S, et al. Histone methyltransferase DOT1L coordinates AR and MYC stability in prostate cancer. *Nat Commun* 2020;**11**:4153.
- Chava S, Bugide S, Edwards YJK, Gupta R. Disruptor of telomeric silencing 1-like promotes ovarian cancer tumor growth by stimulating pro-tumorigenic metabolic pathways and blocking apoptosis. *Oncogenesis* 2021;**10**:48.
- Zhang X, Liu D, Li M, Cao C, Wan D, Xi B, et al. Prognostic and therapeutic value of disruptor of telomeric silencing-1-like (DOT1L) expression in patients with ovarian cancer. *J Hematol Oncol* 2017;**10**:29.
- Song Z, Wei Z, Wang Q, Zhang X, Tao X, Wu N, et al. The role of DOT1L in the proliferation and prognosis of gastric cancer. *Biosci Rep* 2020;**40**:BSR20193515.
- Sun D, Wang W, Guo F, Pitter MR, Du W, Wei S, et al. DOT1L affects colorectal carcinogenesis via altering T cell subsets and oncogenic pathway. *Onc Immunology* 2022;**11**:2052640.
- Chen Y, Liu X, Li Y, Quan C, Zheng L, Huang K. Lung cancer therapy targeting histone methylation: opportunities and challenges. *Comput Struct Biotechnol J* 2018;**16**:211–23.
- Tan AC, Tan DSW. Targeted therapies for lung cancer patients with oncogenic driver molecular alterations. *J Clin Oncol* 2022;**40**:611–25.
- Alexandrova E, Salvati A, Pecoraro G, Lamberti J, Melone V, Sellitto A, et al. Histone methyltransferase DOT1L as a promising epigenetic target for treatment of solid tumors. *Front Genet* 2022;**13**:864612.
- Kim W, Kim R, Park G, Park JW, Kim JE. Deficiency of H3K79 histone methyltransferase Dot1-like protein (DOT1L) inhibits cell proliferation. *J Biol Chem* 2012;**287**:5588–99.
- Campbell JD, Alexandrov A, Kim J, Wala J, Alice H Berger AH, Pedamallu CS, et al. Distinct patterns of somatic genome alterations in lung adenocarcinomas and squamous cell carcinomas. *Nat Genet* 2016;**48**:607–16.
- The Cancer Genome Atlas. Available from: <https://portal.gdc.cancer.gov/>.
- Zhang J, Yang T, Han M, Wang X, Yang W, Guo N, et al. Gain-of-function mutations in the catalytic domain of DOT1L promote lung cancer malignant phenotypes via the MAPK/ERK signaling pathway. *Sci Adv* 2023;**9**:eade9273.
- Chen S, Zhao Y, Liu S, Zhang J, Assaraf YG, Cui W, et al. Epigenetic enzyme mutations as mediators of anti-cancer drug resistance. *Drug Resist Updates* 2022;**61**:100821.
- Yu W, Chory EJ, Wernimont AK, Tempel W, Scpton A, Federation A, et al. Catalytic site remodelling of the DOT1L methyltransferase by selective inhibitors. *Nat Commun* 2012;**3**:1288.
- Deshpande AJ, Chen L, Fazio M, Sinha AU, Bernt KM, Banka D, et al. Leukemic transformation by the MLL-AF6 fusion oncogene requires the H3K79 methyltransferase Dot1l. *Blood* 2013;**121**:2533–41.
- Daigle SR, Olhava EJ, Therkelsen CA, Basavapathruni A, Jin L, Boriack-Sjodin PA, et al. Potent inhibition of DOT1L as treatment of MLL-fusion leukemia. *Blood* 2013;**122**:1017–25.
- Min J, Feng Q, Li Z, Zhang Y, Xu RM. Structure of the catalytic domain of human DOT1L, a non-SET domain nucleosomal histone methyltransferase. *Cell* 2003;**112**:711–23.
- Vlaming H, van Leeuwen F. The upstreams and downstreams of H3K79 methylation by DOT1L. *Chromosoma* 2016;**125**:593–605.

26. De Vos D, Frederiks F, Terweij M, van Welsem T, Verzijlbergen KF, Iachina E, et al. Progressive methylation of ageing histones by Dot1 functions as a timer. *EMBO Rep* 2011;**12**:956–62.
27. Liu T, Xie W, Li C, Ren H, Mao Y, Chen G, et al. Preparation of 5'-deoxy-5'-amino-5'-C-methyl adenosine derivatives and their activity against DOT1L. *Bioorg Med Chem Lett* 2017;**27**:4960–3.
28. Rahman Z, Bazaz MR, Devabattula G, Khan MA, Godugu C. Targeting H3K9 methyltransferase G9a and its related molecule GLP as a potential therapeutic strategy for cancer. *J Biochem Mol Toxicol* 2021;**35**:e22674.
29. Saha N, Muntean AG. Insight into the multi-faceted role of the SUV family of H3K9 methyltransferases in carcinogenesis and cancer progression. *Biochim Biophys Acta Rev Cancer* 2021;**1875**:188498.
30. Takawa M, Masuda K, Kunizaki M, Daigo Y, Takagi K, Iwai Y, et al. Validation of the histone methyltransferase EZH2 as a therapeutic target for various types of human cancer and as a prognostic marker. *Cancer Sci* 2011;**102**:1298–305.
31. Kim KH, Roberts CW. Targeting EZH2 in cancer. *Nat Med* 2016;**22**:128–34.
32. Tan Z, Li T, Lei H, Zhai X. An update on allosteric modulators as a promising strategy targeting histone methyltransferase. *Pharmacol Res* 2021;**172**:105865.
33. Basavapathruni A, Jin L, Daigle SR, Majer CR, Therkelsen CA, Wigle TJ, et al. Conformational adaptation drives potent, selective and durable inhibition of the human protein methyltransferase DOT1L. *Chem Biol Drug Des* 2012;**80**:971–80.
34. Chen C, Zhu H, Stauffer F, Caravatti G, Vollmer S, Machauer R, et al. Discovery of novel Dot1L inhibitors through a structure-based fragmentation approach. *ACS Med Chem Lett* 2016;**7**:735–40.
35. Scheufler C, Möbitz H, Gaul C, Ragot C, Be C, Fernández C, et al. Optimization of a fragment-based screening hit toward potent DOT1L inhibitors interacting in an induced binding pocket. *ACS Med Chem Lett* 2016;**7**:730–4.
36. Möbitz H, Machauer R, Holzer P, Vaupel A, Stauffer F, Ragot C, et al. Discovery of potent, selective, and structurally novel Dot1L inhibitors by a fragment linking approach. *ACS Med Chem Lett* 2017;**8**:338–43.
37. Khirsariya P, Pospíšil P, Maier L, Boudný M, Babáš M, Kroutil O, et al. Synthesis and profiling of highly selective inhibitors of methyltransferase DOT1L based on carbocyclic C-nucleosides. *J Med Chem* 2022;**65**:5701–23.
38. Basavapathruni A, Olhava EJ, Daigle SR, Therkelsen CA, Jin L, Boriack-Sjodin PA, et al. Nonclinical pharmacokinetics and metabolism of EPZ-5676, a novel DOT1L histone methyltransferase inhibitor. *Biopharm Drug Dispos* 2014;**35**:237–52.
39. Bahekar RH, Jadav PA, Goswami AD, Shah HA, Dave BN, Joshi DA, et al. An efficient and scalable synthesis of *tert*-butyl (3*aR*,6*aS*)-5-oxohexahydrocyclopenta[*c*]pyrrole-2(1*H*)-carboxylate: a pharmacologically important intermediate. *Org Process Res Dev* 2017;**21**:266–72.